\$ SUPER

Contents lists available at ScienceDirect

Metabolism

journal homepage: www.journals.elsevier.com/metabolism





Lysine potentiates insulin secretion via AASS-dependent catabolism and regulation of GABA content and signaling

Felipe Muñoz ^a, Qian Gao ^b, Matthias Mattanovich ^b, Kajetan Trost ^b, Ondřej Hodek ^c, Andreas Lindqvist ^a, Nils Wierup ^a, Malin Fex ^a, Thomas Moritz ^{b,*}, Hindrik Mulder ^a, Luis Rodrigo Cataldo ^{a,b,*}

- ^a Lund University Diabetes Centre, Lund University, Malmo, Sweden
- ^b The Novo Nordisk Foundation Centre for Basic Metabolic Research, University of Copenhagen, Copenhagen, Denmark
- ^c Department of Forest genetics and Plant Physiology, Swedish University of Agricultural Sciences, Umeå, Sweden

ARTICLE INFO

Keywords:
Lysine
GABA
Glutamate
GDH
AASS
GABA shunt
Amino acids
Mitochondrial metabolism
TCA cycle
Insulin secretion
Type 2 diabetes

ABSTRACT

Lysine is an essential amino acid with insulinotropic effects in humans. In vitro, it enhances glucose-stimulated insulin secretion (GSIS) in β -cell lines and rodent islets. While lysine is thought to act via membrane depolarization similar to arginine, the role of its intracellular metabolism in β -cell function remains unexplored.

Here, we show that lysine acutely potentiates GSIS and that genes encoding enzymes in the lysine degradation pathway, including AminoAdipate-Semialdehyde Synthase (AASS), a key mitochondrial enzyme catalysing the first two steps of lysine catabolism, were present in human pancreatic islets and INS1 832/13 β cells. Some of these genes including AASS, ALDH7A1, DHTKD1, and HADH, were downregulated in pancreatic islets from type 2 diabetes (T2D) versus non-diabetic (ND) donors. Silencing AASS in human islets and INS1 832/13 β cells led to reduced GSIS. Integrated transcriptomics and metabolomics revealed altered expression of GABA metabolism genes, reduced GABA content and accumulation of glutamate in Aass-KD cells. Mitochondrial TCA cycle and OXPHOS function was impaired, evidenced by decreased ATP/ADP ratio, diminished glucose-stimulated mitochondrial respiration, and elevated lactate/pyruvate ratio. Cytosolic calcium responses to glucose and GABA were also disrupted.

Pharmacological analyses demonstrated that inhibition of GABA synthesis or degradation did not account for the reduced GSIS, but providing substrates and activation of GDH partially restored insulin secretion, pointing to a diminished glutamate supply as a contributing factor. Remarkably, exogenous GABA restored insulin secretion in β cells and human islets with suppressed AASS-dependent lysine catabolism, supporting a role for GABA as both a metabolic substrate and signaling effector.

Together, these findings identify AASS-mediated lysine catabolism as a critical regulator of β -cell metabolic integrity, linking impaired lysine metabolism to GABA depletion, mitochondrial dysfunction, and secretory failure in T2D islets. They also underscore the nutritional importance of essential amino acids such as lysine in sustaining GSIS and glucose homeostasis, and support therapeutic strategies aimed at restoring lysine catabolism or GABA/glutamate balance to maintain β -cell function.

1. Introduction

A recent systematic analysis of insulin secretion dynamics in human

pancreatic islets in response to macronutrients, highlighted the insulinotropic actions of amino acids [1]. Notably, insulin secretion in islets from 9 % of donors was more strongly stimulated by amino acids than by

Abbreviations: GABA, γ-aminobutyric acid; GABA-T, GABA transaminase; GAD, glutamic acid decarboxylase; SSA, succinic semialdehyde; GSIS, glucose-stimulated insulin secretion; AASS, Aminoadipate-semialdehyde synthase; T2D, Type 2 Diabetes; ND, Non-Diabetes; LKR, lysine-ketoglutarate reductase; SDH, saccharopine dehydrogenase; MCF, Metabolic Coupling Factor; ACC, acetyl-CoA carboxylase; IBMX, 3-isobutyl-1-methylxanthine; OCR, oxygen consumption rate; DEGs, differentially expressed genes; GSEA, Gene set enrichment analysis; α -KG, α -ketoglutarate; GDH, Glutamate Dehydrogenase; VRAC, volume-regulated anion channel; α -KIC, α -ketoisocaproic acid; OXPHOS, oxidative phosphorylation; PDE, Pyridoxine-dependent epilepsy; PLP, pyridoxal-5-phosphate.

E-mail addresses: thomas.moritz@sund.ku.dk (T. Moritz), rodrigo.cataldo@med.lu.se (L.R. Cataldo).

^{*} Corresponding authors at: Jan Waldenströms gata 35, SE-21428 Malmö, Sweden.

glucose [1]. This study highlights the necessity of further investigating the mechanisms by which non-glucose nutrients, especially amino acids, influence metabolic responses in human islets and their role in regulating glucose homeostasis.

Lysine is an essential amino acid with established insulinotropic effects in humans for over 50 years [2]. A study administering equal intravenous doses (30 g) of individual amino acids in healthy subjects found that lysine has greater insulinotropic potency than leucine and comparable to arginine [2]. In line with this, the strong insulinogenic index of some dairy food with low glycaemic index has been attributed to raised plasma levels of lysine, arginine and branched chain amino acids [3].

The ability of lysine to directly potentiate insulin secretion in β cells has also been demonstrated by in vitro studies. The potency of amino acids to enhance insulin secretion in the presence of glucose was compared in INS1E cells and mouse islets by administrating equimolar concentrations (10 mM) of each amino acid. Lysine and arginine were the most potent amino acids to enhance GSIS [4].

It is well-established that several amino acids potentiate insulin secretion in the presence of glucose [5]. The mechanisms of action of some amino acids are metabolism-dependent, where they act as energy substrates and increase the production of ATP. The mechanism of other amino acids is metabolism-independent and insulin secretion is potentiated by an electrochemical effect, after depolarizing the plasma membrane via their positively charged properties or upon cotransporting Na $^+$ [5,6]. Due to its positive charge at physiological pH, similar to arginine, it's been assumed for decades that the insulinotropic action of lysine is mediated by its uptake in β cells, leading to plasma membrane depolarization [4]. However, it remains unclear whether the insulinotropic effect of lysine is mediated by an electrochemical action or by a metabolism-dependent mechanism. Furthermore, the potential contribution of lysine catabolism within β cells to the amplification of GSIS has not been investigated.

AminoAdipate-Semialdehyde Synthase (AASS) is a mitochondriallylocated bifunctional enzyme with lysine-ketoglutarate reductase (LKR) and saccharopine dehydrogenase (SDH) activities [7,8], carrying out the first two steps in the saccharopine catabolic pathway of lysine. AASSmediated lysine catabolism may directly potentiate insulin secretion since insulinotropic metabolites such as glutamate and acetyl-CoA are produced along the pathway. Indeed, GC-MS-based labelling experiments have shown that lysine is the precursor for de novo synthesis of up to 33 % of the glutamate pool in the mammalian brain [7]. Glutamate is accumulated in β cells in response to glucose stimulation and enhances GSIS, hence considered a Metabolic Coupling Factor (MCF) [9,10]. Glutamate anaplerotically enters the TCA cycle upon conversion to α -ketoglutarate by the enzyme glutamate dehydrogenase (GDH) [9] or exits mitochondria and is taken up into insulin granules to promote exocytosis [9,11]. In addition, glutamate may represent a route for γ-aminobutyric acid (GABA) provision as glutamate is a direct precursor for GABA synthesis in β cells [12], another important regulator of β cell mass and function [13,14]. On the other hand, acetyl-CoA, an end product of the AASS-dependent lysine catabolism can increase GSIS by feeding carbons into the TCA cycle or be exported from mitochondria to the cytosol as a substrate for acetyl-CoA carboxylase (ACC) to produce malonyl-CoA in the cytosol, another MCF for GSIS [10].

The lysine catabolism pathway holds significant clinical relevance, as epidemiological studies have identified plasma levels of lysine and its metabolites, such as 2-aminoadipic acid, as predictive risk factors for type 2 diabetes (T2D) [15,16]. Furthermore, mutations in genes encoding enzymes involved in this pathway, including AASS, have been implicated in inborn errors of metabolism, such as hyperlysinemia [17,18] (OMIM: 238700). Most of these metabolic disorders are associated with accumulation of toxic levels of metabolites produced along the lysine catabolic pathway. Therefore, AASS-dependent catabolism of lysine may play a dual role in β cell function by maintaining lysine at physiological levels and providing lysine-derived metabolites that

amplifies GSIS.

2. Research design and methods

2.1. Human pancreatic islet cohort

Human pancreatic islets were obtained from the EXODIAB Human Tissue Laboratory, which receives islets from the Nordic Network for Clinical Islet Transplantation (http://www.nordicislets.org). The clinical characteristics of the donors of islets from this cohort (n = 188) and all methodological details related to RNA sequencing of islets have been published [19].

2.2. Cell culture

INS1 832/13 and EndoC- β H1 cells were cultured as previously described [20,21]. EndoC- β H1 cells were cultured in Matrigel/fibronectin-coated (100/2 mg/mL, Sigma-Aldrich) flasks with DMEM containing 5.6 mmol/L glucose, 2 % BSA, 10 mmol/L nicotinamide, 50 mmol/L β -mercaptoethanol, 5.5 mg/mL transferrin, 6.7 ng/mL sodium selenite, 100 IU/mL penicillin, and 100 mg/mL streptomycin at 37 °C in a humidified atmosphere with 5 % CO₂.

2.3. GSIS in β cell lines and human islets

INS1 832/13 cells (1.7 \times 10⁵ cells/cm²) and EndoC- β H1 cells (1.5 \times 10⁵ cells/cm²) were seeded in 24 and 48 well-plates, respectively, 96 h prior to experiments. Seeded cells and human pancreatic islets (10 islets/well, 24-WP, 4-6 replicates/condition) were starved in secretion assay buffer (SAB) buffer (final SAB 1× composition was (in mM): 114 NaCl; 4.7 KCl; 1.2 KH2PO4; 1.16 MgSO4; 20 HEPES; 2.5 CaCl2; 25.5 NaHCO3; 0.2 % bovine serum albumin (BSA), pH 7.2-7.4) with low glucose (LG, 1-2.8 mM mM). Then, cells and islets were simultaneously (in parallel wells) stimulated for 1 h with SAB LG, high glucose (HG, 16.7-20 mM) or HG + 3-isobutyl-1-methylxanthine (IBMX) (100 μ M). The insulin concentration in the supernatants (accumulated during 1 h of stimulation) was measured using the insulin ELISA: for samples from INS1 832/13 cells (non-diluted) High Range Rat Insulin ELISA (Mercodia, catalogue number (#): 10–1145-01), for samples from EndoC- β H1 cells (dilution factor: 12.5) and from human islets (dilution factor: 5) the Human Insulin Elisa (Mercodia, #10-1113-10). The total insulin content was measured in EndoC-βH1 cells and human islets by extraction of total cells/islet protein with RIPA buffer (composition was: 150 mM NaCl, 1 % NP40, 0.5 % sodium deoxycholate, 0.1 % SDS, 50 mM TRIS-HCl, pH 8.0); insulin secretion was normalized to the total insulin content and expressed as % secreted insulin.

2.4. AASS silencing in β cell lines and human islets

INS1 832/13 cells (1.5 \times 10⁵ cells/cm²) were seeded in 24 well plates and transfected after 24 h with 10 nM of scramble negative control (NC) (Thermofisher, custom select siRNA: 5'-GAGACCCUAUCC-GUGAUUAUU-3') or rat Aass siRNA (Thermofisher, #4390771; s150503). EndoC- β H1 cells (1.8 \times 10⁵ cells/cm²) were seeded in 48 well plates and transfected 24 and 48 h after (two successive days, double shot) with 40 nM of Silencer Select Negative Control No. 1 siRNA (Thermofisher, #4390843) or human AASS siRNA (Thermofisher, # 4392420; s19785). Human pancreatic islets (400-500) were seeded in 35 mm petri dish containing 2 mL of RPMI medium (5 mM glucose, 10 % FBS (Sigma #7524), 200 mM L-Glutamine) and transfected on two successive days with 0.5 mL of 50 nM of a Silencer Select Negative Control No. 1 siRNA (Thermofisher, #4390843) or human AASS siRNA (Thermofisher, #4392420; s19785), using Lipofectamine RNAiMAX Transfection Reagent (Thermofisher, #13778075). Details of donors of pancreatic islets used for experiments of AASS silencing are given in Table 1 (Fig. S1A). Human pancreatic islets were cultured as previously

described [22]. All procedures were approved by the Swedish Ethical Review Authority.

2.5. mRNA expression analysis

Total RNA was isolated by RNeasy Mini Kit (Qiagen) and cDNA was generated with RevertAid First-Strand cDNA synthesis kit. Ten ng cDNA/well (in duplicates) were used for qPCR; Aass rat (Rn01455736_m1) and human AASS (Hs00194991_m1) taqman assays were obtained from Thermofisher. qPCR assays were performed using Applied Biosystems QuantStudio7 Flex Real-Time PCR System (Thermofisher). Relative gene abundance was calculated using the $\Delta\Delta$ Ct method with β -actin as reference gene and expressed as fold change to control.

2.6. Western blotting

INS1 832/13 cells were seeded in 12-well plates (1.7 \times 10⁵ cells/ cm²) and transfected with either Aass-targeting or scrambled (negative control) siRNA oligonucleotides (as described above). Human islets were transfected twice with 50 nM siRNA (24 h apart) and lysed 72 h after the second transfection. Both cell types were lysed in RIPA buffer (Pierce, #A32961) supplemented with protease and phosphatase inhibitors. Protein concentrations were quantified using the BCA Protein Assay Kit (Pierce), and 30 µg of total protein per sample was separated on 4-20 % Mini-PROTEAN TGX gels (Bio-Rad) and transferred to PVDF membranes. After blocking in 5 % skim milk in TBST, membranes were incubated overnight at 4 °C with primary antibodies: anti-AASS (Thermo Fisher, #PA5-54262; 0.3 µg/mL) or anti-GDH1/2 (Cell Signaling, ID: 12793; 1:1000). After washing, membranes were incubated with HRP-conjugated secondary antibody (Bio-Rad, ID: 1706516; 1:3000), developed using enhanced chemiluminescence (ECL), and imaged. Densitometric analysis was performed using ImageJ, with stainfree total protein used as the loading control.

2.7. Immunofluorescence staining

Immunofluorescence (IF) staining was performed to assess AASS protein expression in INS1–832/13 cells. Cells (5 imes 10 4 per well) were seeded into poly-D-lysine-coated 8-well glass chamber slides and allowed to adhere for 24 h. Cells were then transfected with either nontargeting control siRNA or Aass-specific siRNA oligonucleotides (as described above). After 48 h, cells were fixed in 4 % paraformaldehyde (PFA) for 15 min at room temperature. Human islets samples from ND an T2D donors were processed according to the tissue preparation procedure previously reported [23]. Following fixation, cells were blocked for 2 h in 5 % normal donkey serum (Jackson ImmunoResearch) supplemented with 1 % bovine serum albumin (BSA) in PBS. Cells were incubated overnight at 4 °C with either an isotype control antibody or anti-AASS primary antibody (Atlas Antibodies, HPA020728) diluted to 1 μg/mL in blocking buffer. The following day, slides were washed three times in PBS and incubated for 2 h at room temperature with a donkey anti-rabbit Alexa Fluor 647-conjugated secondary antibody (Invitrogen, A31573; 1:1000 dilution) together with DAPI (Invitrogen, 1:6000 dilution) for nuclear staining. Samples were stored in mounting media. Images were taken using the Nikon AX-R Confocal Microscope (20× objectives). Images were analyzed using FIJI 1.54p.

2.8. Lactate measurement

INS1 832/13 cells (1.7 \times 10^5 cells/cm²) were seeded in 24 well plates, transfected with scramble (negative control, NC) or $\it Aass$ siRNA (10 nM) (as described in section 2.3) and GSIS determined (as described in section 2.2). The concentration of the extracellular lactate accumulated during 1 h in response to stimulation with SAB buffer (LG or HG) was measured by use of a Lactate Colorimetric/Fluorometric Assay Kit

(Biovision, #607–100) following the manufacturer's instructions. Briefly, cell conditioned samples and lactate standards were mixed with an enzyme plus fluorescent probe mix in a ratio 1:1, incubated for 30 min (at room temperature) and fluorescence emission read (Ex/Em = 535/590 nm) in a microplate reader. Lactate concentrations were normalized by total cell mass in respective wells (protein mass measured by Pierce BCA Protein Assay Kit).

2.9. Metabolomics analysis

The cellular metabolome was analyzed by combined gas chromatography-mass spectrometry (GC-MS) as previously described [24,25]. Briefly, INS1 832/13 cells were stimulated with SAB LG, HG or HG + IBMX for 1 h (as described for GSIS above) and total cellular metabolites extracted with methanol/water $(9/1, \nu/\nu)$ containing a cocktail of stable isotope labelled internal standards (²H₄-succinate (0.22 mg/L), ²H₈valine (4.41 mg/L), ¹³C₄–3-hydroxybutyric acid (2.21 mg/L), ¹³C₅ [15] N-glutamic acid (22.06 mg/L), ²H₁₉-decanoic acid (4.41 mg/L) and ²H₃₁-palmitic acid (22.06 mg/L). Proteins were precipitated by three repeated rounds of shaking/snap freezing on liquid nitrogen, incubation in ice for 1 h and centrifugation. Seven independent experiments were performed. The generated raw data were pre-processed using an inhouse script developed at Swedish Metabolomics Centre, Umeå, Sweden. The detected peaks were identified by comparison of mass spectra and retention indexes using NIST MS Search v.2.0, using in-house and NIST98 spectral databases. After pre-processing and filtering of the metabolites of high coefficient of variation in quality control pool samples (>25 %), levels of 21 metabolites were used for further analysis.

2.10. Mitochondrial oxygen consumption rate (OCR) measurements

OCR was evaluated with a Seahorse XFe24 extracellular flux analyzer (Agilent Technologies). INS1 832/13 cells were transfected with scramble (negative control, NC) or Aass siRNA (10 nM) and cultured for 72 h. Cells were starved in SAB LG (2.8 mM) for 2 h and OCR was measured in SAB (without bicarbonate/HEPES) every 3 min for 90 min. OCR was measured at basal glucose (2.8 mM glucose) and after adding HG (16.7 mM), 5 μ M oligomycin, 4 μ M Carbonyl cyanide p-trifluoromethoxyphenylhydrazone (FCCP), and 1 μ M rotenone/antimycin A. Wave Seahorse Software and an online tool (seahorseanalytics.agilen t.com) were used to analyze data. Non-mitochondrial respiration was subtracted, and OCR data normalized to total protein content, determined by the colorimetric Biuret method (Pierce-BCA Protein Assay Kit, Thermofisher).

2.11. Quantification of whole-cell ATP and ADP

Cellular ATP and ADP levels were quantified by ultra-high performance liquid chromatography-tandem mass spectrometry (UHPLC-MS/ MS). Prior to analysis, the cell extracts were diluted 10 times with MeOH/water $(1/1, \nu/\nu)$ with final concentration of the labelled internal standards (AMP- $^{13}C_{10}^{15}N_5$, ADP- $^{15}N_5$, ATP— $^{13}C_{10}$) of 1 μ M. Separation of the nucleotides was achieved with a 15-min gradient using a iHILIC-(P) Classic column (PEEK, 50×2.1 mm, $5 \mu m$, HILICON, Umeå, Sweden) with mobile phases composed of (A) 10 mM ammonium acetate in water at pH 9.4 and (B) 10 mM ammonium acetate at pH 9.4 in 90 % acetonitrile, both mobile phases were supplemented with 5 µM medronic acid. The flow rate was 0.35 mL/min, and the gradient elution program was set as follows: 0.0 min (85 % B), 5 min (60 % B), 7 min (30 % B), 8 min (30 % B), 9 min (85 % B), 15 min (85 % B). The UHPLC-MS/MS system consisted of an Agilent 1290 UPLC connected to an Agilent 6490 triple quadrupole tandem mass spectrometer (Agilent, CA, USA). Analytes were ionized using electrospray ionization operated in positive ionization mode. The source and gas parameters were set as follows: ion spray voltage 4.0 kV, gas temperature 150 °C, drying gas flow 11 L/min, nebulizer pressure 20 psi, sheath gas temperature 325 °C, sheath gas

flow rate 12 L/min, fragmentor 380 V. Multiple reaction monitoring (MRM) transitions for AMP, ADP, ATP, and their respective labelled internal standards were optimized by flow injection analysis. Quantification of AMP, ADP, and ATP was conducted based on internal standard calibration. Calibration curves were linear from 5 nM to 50 μM . The accuracy, determined through spiking experiments of the cell extracts (n = 4) with 10 μM standards, was within the acceptable range of 100 \pm 15 %.

2.12. Quantification of extracellular GABA and glutamate

Cellular GABA and glutamate levels were quantified by ultra-high performance liquid chromatography-tandem mass spectrometry (UHPLC-MS/MS). 100 μL of cellular extracts including 100 ng of norvaline as internal standard was evaporated to dryness. Extracted samples were derivatized by AccQ-Tag^TM (Waters, Milford, MA, USA) according to the manufacturer's instructions. Briefly, the dry extract was dissolved in 20 μL 20 mM HCl, 60 μL of AccQ+Tag Ultra Borate buffer and 20 μL of the freshly prepared AccQ+Tag derivatization solution and the sample was immediately vortex for 30s.

Samples were kept at room temperature for 30 min followed by 10 min at 55 °C. The quantification of the amino acids was achieved on the liquid chromatography-tandem mass spectrometer consisting of a Waters Acquity UPLC I-Class connected to a Waters Xevo TQ-XS tandem mass spectrometer (Waters, Manchester, UK). The separation was performed by injecting 1 µL of each sample to an Acquity UPLC BEH C18 column (100 \times 2.1 mm, 1.7 μ m, Waters, MA, USA). The mobile phase consisted of (A) 0.1 % formic acid and (B) acetonitrile with 0.1 % formic acid and was delivered on the column by a flow rate of 0.50 mL/min with the following gradient: The initial conditions consisted of 0.1 % B, and the following gradient was used with linear increments: 0.54-3.50 min (0.1–9.1 % B), 3.50–7.0 (9.1–17.0 % B), 7.0–8.0 (17.0–19.70 % B), 8.0-8.5 (19.7 % B), 8.5-9.0 (19.7-21.2 % B), 9.0-10.0 (21.2-59.6 % B), 10.0-11.0 (59.6-95.0 % B), 11.0-11.5 (95.0 % B), 11.5-15.0 (0.1 % B). Column and autosampler were thermostated at 55 °C and 4 °C, respectively. Analytes were ionized in an electrospray ion source operated in the negative mode. The source and gas parameters were set as follows: ion spray voltage 3.5 kV, desolvation temperature 300 $^{\circ}\text{C},$ desolvation gas flow 800 L/h, nebulizer pressure 7 Bar, cone gas flow 150 L/h. The instrument was operated in multiple reaction monitoring mode (MRM), and dwell time was set to 30 ms for all transitions. For quantification 8points calibration curves were used including different levels of nonlabelled and constant levels of the labelled nor-valine internal standard. The instrument was controlled by MassLynx 4.2, and data processing was performed with TargetLynx XS (Waters, MA, USA).

2.13. mRNA sequencing analysis

Messenger RNA sequencing (mRNAseq) was performed by the Single-Cell Omics platform (SCOP) at the Novo Nordisk Foundation Centre for Basic Metabolic Research. Total RNA was isolated using the RNeasy Mini Kit (Qiagen) according to manufacturer's protocol from NC and Aass-KD INS1 832/13 cells. Total RNA was treated with DNAse and delivered to the SCOP where they performed RNA quality control analysis (20 ng of RNA) and prepared RNA-seq library (250 ng of RNA). Libraries were prepared using the Universal Plus mRNA-seq protocol (Tecan, CH) as recommended by the manufacturer. Libraries were quantified with NuQuant using the CLARIOstar Plate Reader (BMG Labtech, DE), quality checked using a TapeStation instrument (Agilent Technologies, US) and subjected to 52-bp paired-end sequencing on a NovaSeq 6000 (Illumina, US).

For the RNAseq data analysis, the nf-core [26] RNA-seq pipeline was used to align RNA-seq reads against the rat genome assembly and <code>Aass</code> transcripts [27]. Testing for differential expression was performed using edgeR [28] v.3.38.4, using the quasi-likelihood framework with a fitted model of the form $\sim\!0+$ group, where group encoded both genotype and

treatment. Contrasts were constructed as described in the edgeR manual. Gene Ontology [29] and Reactome [30] enrichments were found using the CAMERA function [31] which is part of the edgeR package. Only gene ontologies with between 5 and 500 genes were investigated.

2.14. Statistical analysis

Data are shown as mean \pm SEM of at least three independent experiments. Differences between two groups were assessed using the Student's t-test for normally distributed data or the Mann–Whitney test for non-parametric data. Comparisons among multiple groups were performed using ANOVA. Statistical significance was set at p < 0.05. SPSS 28 and Prism 9.0 (GraphPad) were used for correlational and basic statistical analysis and graph generation. For metabolomics data, batch effects were removed using ComBat [32] and data expressed as cell content concentration (μM) for each metabolite at LG and HG or as ratio of specified metabolite cell contents. ANOVA was applied for identifying differentiating metabolites between two genotypes and p values were corrected for multiple testing with the Benjamini-Hochberg procedure. Prior to multivariate analysis, data were mean-centered and scaled to unit variance to ensure equal weight of all metabolites in analysis. Unsupervised principal component analysis (PCA) was first used to recognize underlying patterns and to detect outliers. Supervised orthogonal partial least-squares discriminant analysis (OPLS-DA) was then performed to find discriminating metabolites based on the variable importance on projection (VIP) score. The VIP measures the influence of metabolites on the predictive component in the model, in other words; how much influence the metabolite has on discriminating the two different genotypes (Aass-KD vs NC control). Metabolites with VIP score > 1 were considered metabolites responsible for the separation between the two genotypes. The OPLS-DA model was validated with 3-fold crossvalidation and permutation test (n = 200). All the metabolomics analysis was carried out in R 4.1.2. Pathway enrichment analysis was performed with MetaboAnalyst based on the Kyoto Encyclopedia of Genes and Genomes (KEGG) library using hypergeometric test.

3. Results

3.1. Effects of lysine on insulin secretion in INS1 832/13 β cells and human pancreatic islets

Intravenous administration of lysine in healthy subjects has insulinotropic effects [2] and direct stimulation of INS1E cells and mouse islets with lysine enhances GSIS [4]. Therefore, we first aimed to test whether lysine also has direct insulinotropic effects in vitro in the glucose-responsive β cell line INS1 832/13 and in human pancreatic islets.

We observed a significant lysine-promoted increase (+33 %) in insulin secretion in the presence of high glucose (HG) (214.9 \pm 117.6 vs. 285.6 \pm 125.7 ng/mg of protein/h, *p*-value<0.0001), but no effects on the presence of low glucose (LG) in INS1 832/13 β cells (Fig. 1A).

Similarly, in islets from non-diabetic (ND) donors, acute stimulation with lysine (10 mM) had no effect on insulin secretion at LG, but increased insulin secretion by an average of 22 % at HG (6.4 \pm 3.2 vs. 7.79 \pm 3.9 % of content, p-value: 0.0088) (Fig. 1B). We also evaluated the effects of lysine on GSIS by calculating the stimulatory index (the ratio of insulin secretion at HG versus LG) in the presence or absence of lysine. We found an average of 30 % increase (p=0.039) in the stimulatory index when islets were stimulated in the presence of lysine (Fig. 1C).

When same type of experiments was conducted in pancreatic islets from T2D patients, we observed no significant changes in GSIS in the presence vs. absence of lysine (Fig. 1D, E).

Therefore, these data indicates that lysine potentiates insulin secretion in a glucose dependent manner in INS1 832/13 cells and in healthy

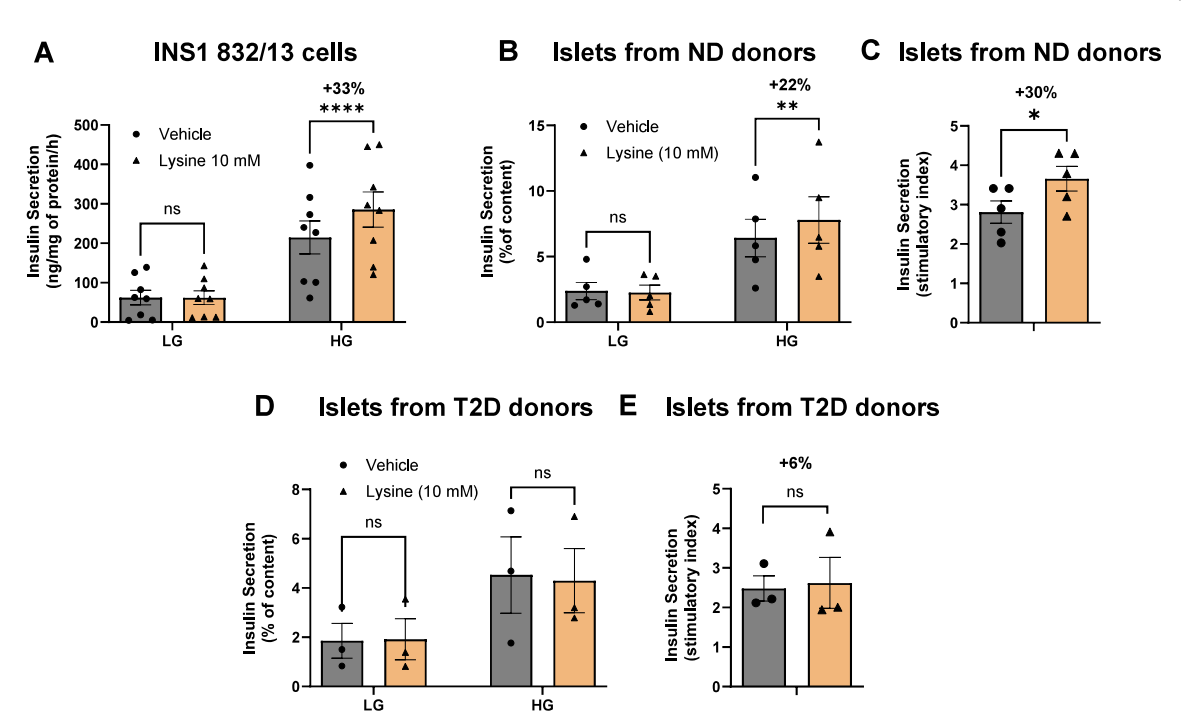


Fig. 1. Effects of lysine on insulin secretion in INS1 832/13 β cells and in human pancreatic islets. **A.** Insulin secretion at LG and HG in presence and absence of lysine (10 mM) in INS1 832/13 β cells (n = 8). **B, E.** Insulin secretion in human pancreatic islets from ND (n = 5) (**A**) and T2D (n = 3) (**D**) donors at low glucose (LG, 2.8 mM) and high glucose (HG, 16.7 mM) in the absence and presence of lysine (10 mM). **C, E.** Calculated lysine-provoked stimulatory index (insulin secretion at HG/LG in presence vs absence of lysine) in ND (**C**) and T2D (**E**) islets. All graphs show individual data points and mean ± s.e.m. Statistical tests: Two-way ANOVA (A, B, D), Student *t*-test (C, E). *p < 0.05, *p < 0.05, *p < 0.01, ****p < 0.001, ****p < 0.0001. ND, non-diabetic; T2D, type 2 diabetes.

pancreatic islets but not in islets from T2D donors.

3.2. Expression of lysine catabolism pathway genes is reduced in pancreatic islets from T2D donors, and AASS expression levels are associated with islet function

To investigate the relevance of the lysine catabolism pathway in β cell metabolism and insulin secretory function, and whether dysregulation of this pathway contributes to β cell dysfunction in T2D, we examined the expression of genes encoding the enzymes involved in lysine catabolism (see pathway chart in Fig. 2F) in pancreatic islets from ND and T2D donors (Fig. 2A-E). Interestingly, we found that expression of AASS (steps 1 and 2), ALDH7A1 (step 3), AADAT (step 4), DHTKD1 (step 5), and HADH (step 8) was reduced in pancreatic islets from T2D compared to ND donors (Fig. 2A-E). Notably, mRNA expression levels of ALDH7A1 and DHTKD1 were highly correlated with AASS expression in pancreatic islets (Fig. S1B, C), suggesting a common regulatory mechanism for lysine catabolism pathway genes.

We also assessed AASS protein expression in pancreatic islets from ND and T2D donors, using immunostaining (Fig. S1D). We confirmed the presence of AASS protein in human pancreatic β cells as AASS and INSULIN staining colocalized (Fig. S1D). This is consistent with published transcriptomic data from FACS-sorted human pancreatic islet cells, showing significantly higher AASS mRNA expression in $\boldsymbol{\beta}$ cells than in α cells (310 \pm 56 vs. 147 \pm 39 normalized counts, q-value: 6e-15) [33]. This finding also aligns with a strong correlation between AASS protein expression and β cell proportion in human islets (Fig. S1E) (data obtained from www.humanislets.com) [72]. Notably, mass spectrometry-based proteomic analysis revealed a significant reduction in AASS protein abundance in T2D islets compared to ND islets (Fig. S1F) (www. humanislets.com) [72]. Additionally, protein levels of other components of the AASS-dependent lysine catabolic pathway, including GCDH (adj. p = 0.00537), ECHS1 (adj. p = 0.0539), and HADH (adj. $p = 9.41 \times 10^{-5}$ 10⁻¹²), were reduced in T2D compared to ND islets (www.humanislets. com) [72]. The roles of these enzymes within the lysine catabolic pathway are depicted in Fig. 2F.

Since AASS encodes the enzyme responsible for the first two ratelimiting steps in the lysine catabolism pathway [17], we focused on AASS expression as the key regulator of lysine catabolism. To gain insight into the potential role of AASS-dependent lysine catabolism in human islet function and glucose homeostasis, we evaluated the association between AASS mRNA expression in islets and their ex vivo GSIS, glycemic control (HbA1c), and donor BMI. We found that AASS mRNA levels were positively correlated with GSIS (the stimulatory index, SI) (Fig. 2G), but did not correlate with HbA1c (Fig. 2H) or with BMI (Fig. 2I). Importantly, in an independent cohort of human islets (www. humanislets.com), we confirmed a positive correlation between AASS protein abundance in human islets and GSIS (in response to both 6 or 15 mM glucose) (Fig. S1G, H) and a negative correlation between AASS protein abundance and donor HbA1c (Fig. S1I). These findings indicate that AASS expression in human islets positively correlates with GSIS capacity and contributes to glucose homeostasis.

To further explore the former association, we evaluated whether AASS mRNA levels were linked to dynamic GSIS function in islets from ND donors (Fig. 2J). We found a positive correlation between AASS mRNA levels and total insulin secretion (Fig. 2K), as well as with insulin secretion during the 1st phase (Fig. 2L) and 2nd phase (Fig. 2M) of dynamic GSIS.

To further assess the contribution of AASS expression to insulin secretory function in human islets, we compared dynamic GSIS between islets from ND donors in the highest (top decile (T.D.), n=16) and lowest (bottom decile (B.D.), n=16) AASS mRNA expression groups (Fig. 2N). We observed that pancreatic islets with the B.D. of AASS expression exhibited reduced insulin secretion during a GSIS perifusion assay (90 min) compared to islets with the T.D. AASS expression (Fig. 2O). The average AUC of insulin secretion during the glucose stimulation period (48–90 min) (Fig. 2P) and throughout the entire assay (48–120 min) (Fig. 2Q) was nominally lower in islets with the B.D. compared to T.D. AASS expression.

Collectively, these findings suggest that reduced AASS expression,

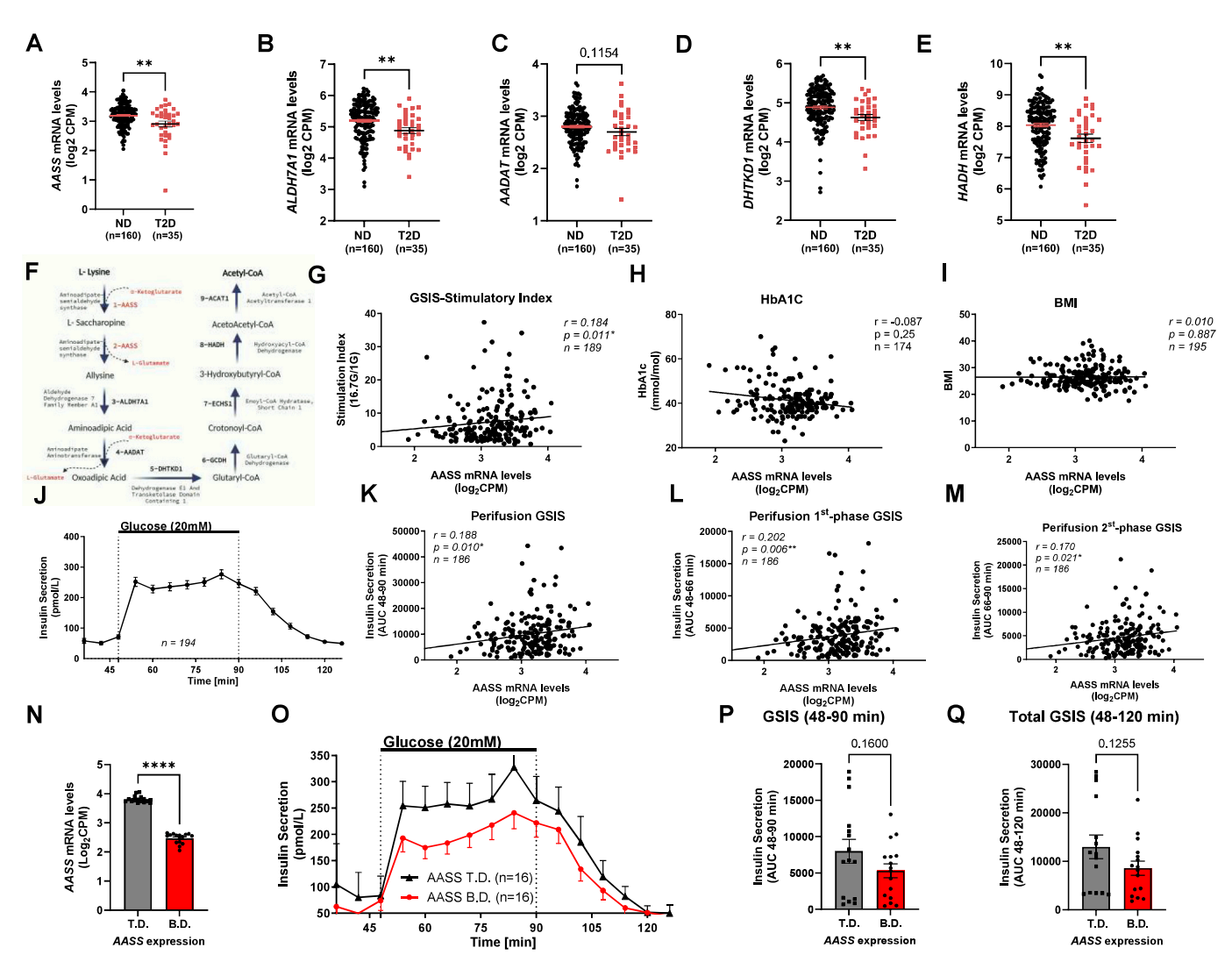


Fig. 2. The Expression of Lysine Catabolism Pathway Genes Is Reduced in Pancreatic Islets from T2D Donors, and AASS Expression Levels Are Associated with Islet Function. **A-E.** mRNA levels of lysine catabolism pathway genes in pancreatic islets from ND (n=160) vs. T2D (n=35) donors. **F.** Scheme illustrating the Saccharopine, AASS-dependent lysine catabolism pathway. **G-I.** Spearman rank correlation analyses between *AASS* mRNA levels in islets and **(G)** GSIS stimulatory index (SI), **(H)** donors HbA1c and **I)** donors BMI. **J-M.** Perifusion dynamic GSIS analysis of human islets. **J.** Average dynamic GSIS trace in human pancreatic islets from ND and T2D donors. **K-M.** Spearman rank correlation analyses between *AASS* mRNA levels in islets and **(K)** AUC of total dynamic GSIS, **(L)** AUC of the first-phase GSIS, and **(M)** AUC of the second-phase GSIS. **N.** Average *AASS* mRNA levels in pancreatic islets from ND donors in the lowest decile (B.D.) vs. the highest decile (T.D.). **O.** Traces and **(P, Q)** Averages AUC of dynamic GSIS in islets from ND donors with the B.D. (n=16) vs. the T.D. (n=16) *AASS* mRNA levels. All graphs show individual data points and mean \pm s.e.m. Statistical tests: Mann-Whitney (A-E), Rank Spearman (G-I, K-M), Student t-test (N, P, Q). *p < 0.05, **p < 0.01, ***p < 0.001, ****p < 0.0001. AASS, Aminoadipate-Semialdehyde Synthase; AUC, area under the curve; GSIS, glucose-stimulated insulin secretion; ND, non-diabetic; T2D, type 2 diabetes.

and the consequent impairment of lysine catabolism in human islets, may contribute to the loss of GSIS in healthy donors and precede β -cell dysfunction and impaired glucose homeostasis in T2D.

3.3. Suppressing AASS-dependent lysine catabolism reduces GSIS in pancreatic islets and INS1 832/13 β cells

To investigate whether the insulinotropic effect of lysine depends on lysine catabolism, we genetically inhibited AASS-dependent lysine catabolism in INS1 832/13 cells and assessed the effects of lysine on GSIS. Aass expression was silenced in INS1 832/13 cells, and efficient knockdown was confirmed at the mRNA by qPCR (Fig. S2A) and at protein levels by Western blot (Fig. S2B-C) and immunocytochemistry analysis (Fig. S2D). We then evaluated the effects of lysine on GSIS in control (NC) versus Aass-knockdown (Aass-KD) cells. While lysine increased insulin secretion in the presence of high glucose (HG) in both NC and Aass-KD cells (Fig. 3A), the stimulatory index (fold change of

insulin secretion at HG vs. LG) in the presence of lysine increased only in NC cells and not in Aass-KD cells (SI in NC cells: 3.5 ± 1.7 (wo lysine) vs. 4.4 ± 1.9 (with lysine), p-value: 0.0127) (Fig. 3B).

Next, we tested whether suppressing AASS-dependent lysine catabolism eliminated the insulinotropic effect of lysine in human islets from ND donors. Reduced *AASS* mRNA and protein expression in human islets was confirmed by qPCR (Fig. S2E) and western blot analysis (Fig. S2F-G), respectively. We measured insulin secretion in response to glucose in the presence or absence of lysine in NC versus *AASS*-KD islets (Fig. 3C). Lysine potentiated insulin secretion in control NC islets but not in *AASS*-KD islets (Fig. 3C). Similarly to INS1 cells, the stimulatory index was increased in NC islets (+42 %) but remained unchanged in *AASS*-KD islets (Fig. 3D).

In a set of independent experiments, we examined whether suppressing AASS-dependent lysine catabolism affected GSIS in islets from ND donors. We observed no differences at LG but a significant reduction of insulin secretion in response to HG stimulation following AASS

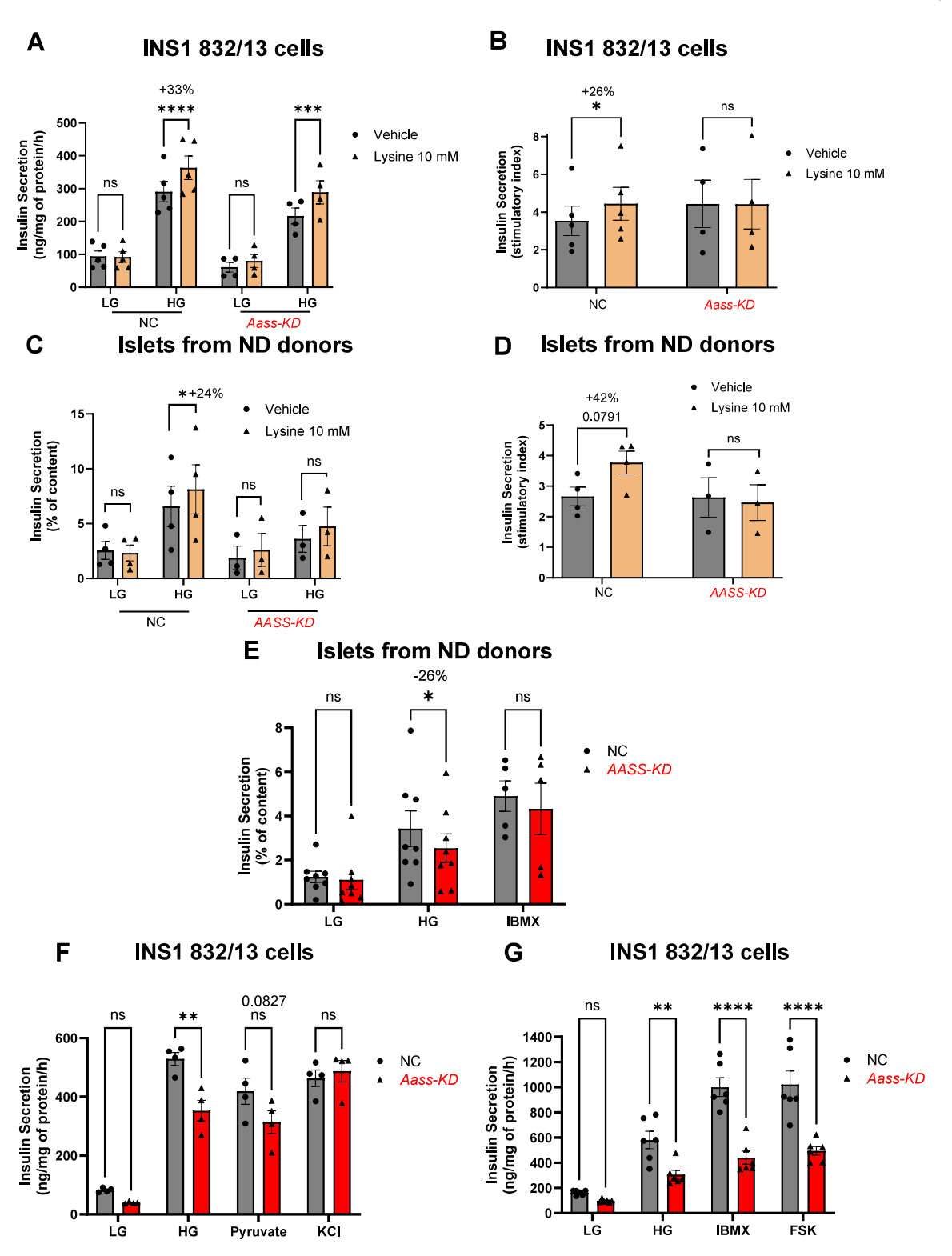


Fig. 3. Suppressing AASS-dependent Lysine Catabolism Reduces Insulin Secretion in Pancreatic Islets and INS1 832/13 β Cells. **A.** Insulin secretion at LG and HG in the absence and presence of lysine (10 mM) in normal control (NC) and *Aass-KD* INS1 832/13 β cells (n=5). **B.** Calculated stimulatory index (insulin secretion at HG/LG) in presence vs absence of lysine in NC and *Aass-KD* INS1 832/13 β cells (n=5). **C.** Insulin secretion in human islets from non-diabetic donors (ND) at low glucose (LG, 2.8 mM) and high glucose (HG, 16.7 mM) in the absence and presence of lysine (10 mM) in control (NC) and *AASS-KD* ND islets (n=4). **D.** Calculated stimulatory index (insulin secretion at HG/LG) in presence vs absence of lysine in NC control and *AASS-KD* ND islets (n=4). **E.** Insulin secretion at LG, HG and HG + IBMX (100 μM) in NC control and *AASS-KD* INS1 832/13 β cells (n=4). **G.** Insulin secretion at LG, HG, HG + IBMX (100 μM) and HG + FSK (10 μM) in NC control and *Aass-KD* INS1 832/13 β cells (n=6). All graphs show individual data points and mean \pm s.e.m. Statistical tests: Two-way ANOVA (A-G). *p < 0.05, **p < 0.01, ***p < 0.001, ****p < 0.0001. AASS, Aminoadipate-Semialdehyde Synthase; KD, knockdown; NC, normal control; ND, normal donor; FSK, forskolin; IBMX, isobutyl-1-methylxanthine.

silencing in human islets (Fig. 3E). No significant change in the amplification effect of IBMX on GSIS was observed between NC and *AASS*-KD islets (Fig. 3E).

The effect of AASS silencing on GSIS was also evaluated in human EndoC- β H1 β cells, where no significant changes were observed (Fig. S3A). This may be attributed to the fetal phenotype of these cells [34].

To further confirm whether selective suppression of AASS-dependent lysine catabolism in β cells impacts GSIS, we assessed insulin secretion in response to various metabolic and pharmacologic stimuli in NC and Aass-KD INS1 832/13 β cells (Figs. 3F, G). Silencing Aass expression did not changed insulin secretion at LG whereas resulted in significantly reduced insulin secretion at HG (529.1 \pm 44.3 vs. 353.0 \pm 70.5 ng/mg of protein/h, p-value: 0.0016) and borderline decreases in response to pyruvate stimulation, but not in response to plasma membrane depolarization with high K $^+$ (Fig. 3F). These data suggest that AASS-dependent lysine catabolism contributes to insulin secretion via a mechanism upstream of plasma membrane depolarization likely involving mitochondrial energy metabolism.

The incretin hormone GLP1 amplifies GSIS by promoting cAMP accumulation upon activation of GLP1 receptor [35]. INS1 832/13 cells respond poorly to the GLP1R agonists; GLP1 or Exendin-4 [20,36]. Thus, to mimic GLP1R activation, IBMX and forskolin (FSK) were used to trigger cAMP accumulation. IBMX and FSK strongly amplified GSIS in NC cells, but this effect was abolished in *Aass*-KD cells (Fig. 3G).

The apparent discrepancy in the effect of silencing AASS on IBMX-induced GSIS between human islets and INS1 cells may reflect paracrine interactions in intact islets, particularly somatostatin release from δ -cells in response to cAMP elevation (with IBMX and FSK). Somatostatin inhibits insulin secretion via SSTR2 receptors on β cells [37], potentially overriding IBMX-induced stimulation and masking the intrinsic β -cell defects upon AASS silencing.

Overall, these data indicate that an active AASS-dependent lysine catabolism contributes to both the lysine-promoted GSIS and to GSIS itself in human pancreatic islets and β cells.

3.4. Transcriptomics and metabolomics analysis suggest a link between AASS-dependent lysine catabolism and GABA content/signaling in β cells

To explore the molecular mechanisms by which AASS-dependent lysine catabolism contributes to GSIS, we performed bulk RNA sequencing (RNAseq) and mass-spectrometry-based metabolomics profiling of NC and *Aass-*KD INS1 832/13 cells (Fig. 4).

The RNAseq analysis revealed that inhibiting AASS-dependent lysine catabolism strongly impacted global gene expression, with 6431 differentially expressed genes (DEGs) in Aass-KD vs. NC cells. Of these, 3202 DEGs were downregulated, while 3229 were upregulated (Fig. 4A). Gene set enrichment analysis (GSEA) highlighted the profound effect of blocking AASS-dependent lysine degradation on overall β cell metabolism (the pathway with the highest false discovery rate (FDR)). Other pathways significantly affected in Aass-KD vs. NC cells included neurodegeneration, endocytosis, Alzheimer's disease, branched-chain amino acid metabolism, autophagy, insulin signaling, long-term potentiation, and insulin secretion, all of which are relevant to β cell physiology (Fig. 4B).

As expected, the RNAseq analysis confirmed a reduction (~70 %) in Aass expression in Aass-KD cells (Fig. 4C). Supporting the idea that silencing Aass resulted in inhibition of the AASS-dependent lysine catabolism pathway [17], the expression of downstream genes in the lysine degradation pathway was also reduced in Aass-KD vs. NC cells, including Aadat (step 4), Echs1 (step 7), Hadh (step 8), and Acat2 (step 9) (Fig. 4C, D).

To evaluate whether inhibiting lysine degradation at downstream steps also affects insulin secretion, we focused on DHTKD1, the enzyme carrying over the step 5 of AASS-dependent lysine catabolism pathway (Fig. 4D), and whose expression, as shown above, is also downregulated

in T2D islets (Fig. 2D). Thus, we silenced the expression of *Dhtkd1* in INS1 832/13 cells and tested its effect on GSIS. We observed a nominal (*p*-value: 0.07) decreased GSIS (Figs. S3B, C).

To evaluate the translational relevance of the transcriptional changes induced by *Aass* silencing in INS1 cells to human β cell dysfunction in T2D, we analyzed the overlap between differentially expressed genes (DEGs) in *Aass*-KD cells and the 395 DEGs we previously identified in pancreatic islets from T2D donors [33].

Remarkably, 33 % (129 genes) of the DEGs in T2D islets were also DEGs in Aass-KD vs. control cells (Fig. S3D). Several of these overlapping DEGs are known regulators of β cell physiology and T2D pathogenesis (Fig. S3E) [36,38], highlighting the critical role of AASS-dependent lysine catabolism in maintaining β cell metabolic integrity and its disruption in T2D-related dysfunction.

We also conducted mass spectrometry-based metabolomics analysis upon silencing of Aass in INS1 832/13 cells (Aass-KD vs. NC cells) in response to glucose and glucose+IBMX stimulation. As expected, principal component analysis (PCA) showed clear separation of metabolic clusters based on glucose stimulation (HG vs. LG) and glucose+IBMX, with a less evident separation based on genotype (Aass-KD vs. NC cells, Fig. 4E). OPLS-DA was then used to identify the metabolites driving variance between Aass-KD and NC cells (Fig. 4F). Strikingly, GABA and glutamate emerged as top metabolites explaining the variation between genotypes. This suggests that suppression of AASS-dependent lysine catabolism may impact a metabolic pathway involving glutamate and GABA, which could account for the loss of GSIS potentiation. Other significant metabolites related to glycolysis (lactate, pyruvate) and the TCA cycle (succinate, fumarate, malate, aspartate, citrate and α -ketoglutarate) also drove variation between Aass-KD and NC cells (Fig. 4F). Multivariate ANOVA confirmed significantly elevated glutamate content and reduced GABA content in Aass-KD vs. NC cells (Fig. 4G).

Metabolomic analysis further confirmed intracellular lysine accumulation in *Aass*-KD cells (Fig. S3F), providing additional evidence of effective genetic suppression of the AASS-dependent lysine catabolism. However, the saccharopine pathway (AASS-dependent) in the mitochondrial matrix is not the only route for lysine degradation. The alternative pipecolic pathway, which occurs in the cytosol and peroxisome [17], may buffer the excess lysine accumulation when AASS-dependent catabolism is suppressed (see pathway chart in Fig. S3G). We therefore examined the expression of genes in the alternative pipecolic pathway in *Aass*-KD. Interestingly, we observed an upregulation of *Crym/KR* and *Pipox*, which encode enzymes for steps 2 and 3 of the pipecolic pathway (step 1 gene is unknown), in *Aass*-KD vs. NC cells (Fig. S3H).

To further investigate the relevance of lysine catabolism for GSIS and whether the pipecolic pathway also contributes to GSIS, we silenced *Aass* alone, *Crym/KR* alone, or both *Aass and Crym/KR* in INS1 832/13 cells. Indeed, silencing each pathway individually reduced GSIS, but simultaneous suppression of both pathways led to an additional reduction of GSIS (Fig. S3I).

3.5. Silencing of AASS results in reduced GABA content, altered GABA shunt and GABA signaling

To gain insights about the molecular mechanism by which AASS-dependent lysine catabolism potentiates GSIS in β cells, we focused on metabolomic data identifying GABA and glutamate as key metabolites differentiating Aass-KD from control cells. We compared glutamate and GABA cell content in Aass-KD and NC cells in response to glucose stimulation (Fig. 5A, B). We observed a trend toward increased glutamate levels (Fig. 5A), while GABA cell content significantly decreased in both basal and glucose-stimulated conditions (Fig. 5B).

Since glutamate can be converted into GABA in a single step by the enzyme glutamate decarboxylase (GAD), we calculated the GABA-to-glutamate ratio. Interestingly, in control β cells, the GABA-to-glutamate ratio decreased in response to glucose stimulation (Fig. 5C),

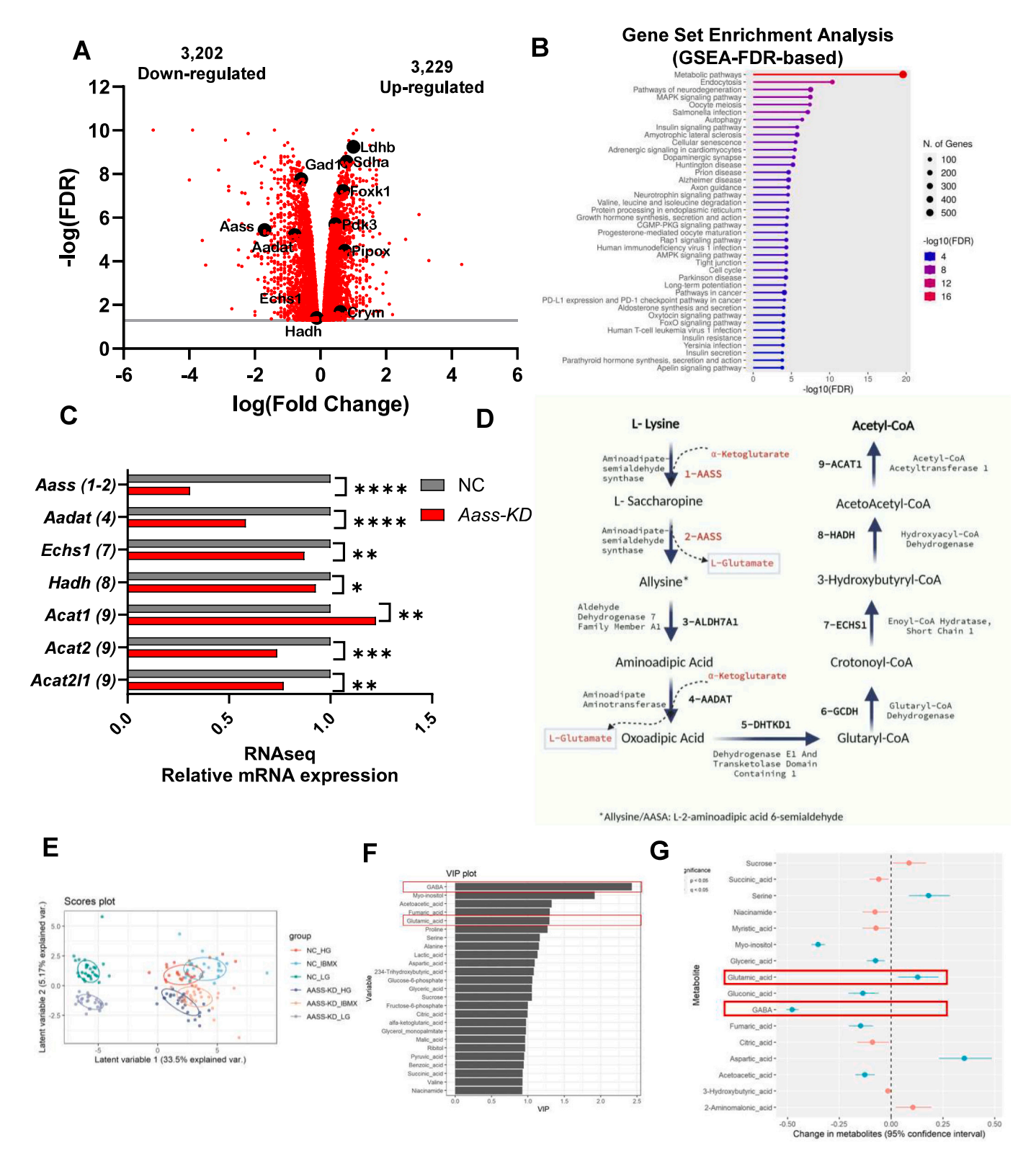


Fig. 4. Transcriptomics and Metabolomics Analysis Suggest a Link Between AASS-Dependent Lysine Catabolism and GABA Content/Signaling in β Cells. **A.** Volcano plot and **B.** GSEA based on data from RNAseq analysis of NC and *Aass*-KD INS1 832/13 β cells (n=4). **C.** Expression levels of lysine catabolism pathway-related genes in NC and *Aass*-KD INS1 832/13 β cells (n=4). **D.** Chart of the lysine catabolism pathway. **E.** PCA score plot showing first two components. **F.** VIP from the predictive component of the OPLS-DA model. **G.** Multivariate ANOVA plot based on data from metabolomics analysis of NC and *Aass*-KD INS1 832/13 β cells (n=7). *p<0.05, **p<0.01, ****p<0.001. ****p<0.0001. GSEA, Gene set enrichment analysis; KD, knockdown; NC, normal control; PCA, principal component analysis; OPLS-DA, orthogonal partial least squares discriminant analysis. Further description of statistical analyses for omics data described in the Methods section.

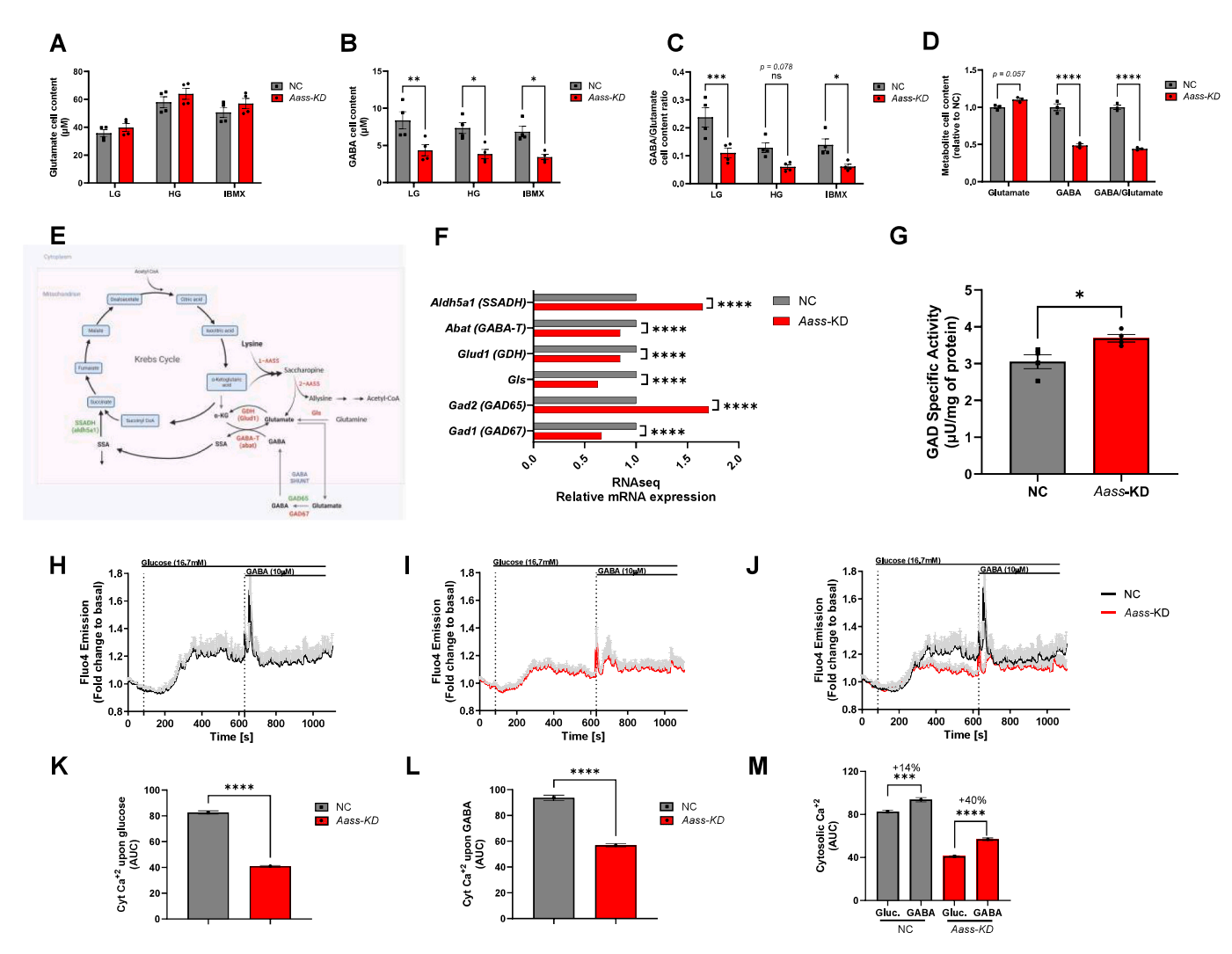


Fig. 5. Silencing of AASS Results in Reduced GABA content, altered GABA Shunt and GABA Signaling. **A.** Glutamate cell content, **B.** GABA cell content and **C.** Calculated GABA to Glutamate Cell content ratio from mass spectrometry-based measurement of metabolites in NC control and *Aass*-KD INS1 832/13 β cells (n = 4). **D.** Glutamate, GABA and GABA/Glutamate cell content at HG based on targeted metabolomics (n = 3). **E.** Chart of GABA shunt pathway, highlighting DEGs in *Aass*-KD vs. NC INS1 832/13 β cells, in green upregulated genes, in red, downregulated genes. **F.** Expression levels of GABA shunt-related genes in NC control and *Aass*-KD INS1 832/13 β cells (n = 4). **H-M.** Average traces of live-cell calcium imaging in response to glucose (16.7 mM) and GABA (10 μM) stimulation in **H.** NC control and **I.** *Aass*-KD INS1 832/13 β cells. **J.** Comparison of the calcium traces in NC vs *Aass*-KD cells (n = 6). Average AUC of **K.** glucose-stimulated and L. GABA calcium responses and **M.** their comparison in NC vs. *Aass*-KD INS1 832/13 β cells. All graphs show individual data points and mean \pm s.e.m. Statistical tests: Two-way ANOVA (A-F), Student *t*-test (G, K-M). *p < 0.05, *p < 0.01, ***p < 0.001, ****p < 0.0001. GABA, γ-aminobutyric acid; GAD, glutamic acid decarboxylase; KD, knockdown; NC, normal control. (For interpretation of the references to colour in this figure legend, the reader is referred to the web version of this article.)

which aligns with previous studies showing that glucose and others secretagogues stimulates glutamate production [39] and GABA catabolism to enhance insulin secretion [40]. Notably, *Aass*-KD cells exhibited a marked reduction in the GABA-to-glutamate ratio under both basal and glucose-stimulated conditions compared to control cells (Fig. 5C). In a set of independent targeted metabolomics experiments, we further confirmed reduced GABA content and GABA-to-glutamate ratio at HG in *Aass*-KD cells (Fig. 5D).

These findings suggest that suppression of AASS-dependent lysine catabolism may impair the supply of glutamate within the mitochondrial matrix, thereby disrupting glucose-stimulated glutamate- and GABA-related metabolic pathways. In Aass-KD cells, reduced lysine catabolism could lead to diminished GABA synthesis due to limited glutamate availability or reduced GAD activity. Alternatively, impaired lysine degradation may enhance GABA catabolism through increased GABA shunt activity, resulting in decreased intracellular GABA levels.

In the GABA shunt pathway, α -ketoglutarate (α -KG) from the TCA

cycle is transaminated with GABA via GABA transaminase (GABA-T) to produce glutamate and succinic semialdehyde (SSA) in the mitochondrial matrix. Glutamate can then exit the matrix to the cytosol, where it can be converted back into GABA via GAD [40,41] (see scheme in Fig. 5E).

Alongside the marked reduction in the GABA-to-glutamate ratio in Aass-KD cells, we observed altered expression of several genes related to the GABA shunt pathway, including gls (Glutaminase), abat (GABA-T), glud1 (Glutamate Dehydrogenase 1, GDH), and aldh5a1 (SSADH), as well as gad1 (GAD67) and gad2 (GAD65) (Fig. 5F). Interestingly, in line with the reduced expression of gls and abat in Aass-KD cells, we observed a positive correlation between the expression of AASS and ABAT (Fig. S4A) and AASS and GLS (Fig. S4B) in human islets, suggesting that the expression of GABA shunt genes may be regulated by the activity of the AASS-dependent lysine catabolism in human β cells.

To explore whether the GABA shunt pathway is relevant to T2D islet dysfunction, we also examined the expression of GABA shunt genes in pancreatic islets from T2D vs. ND donors. We found downregulation of ABAT (Fig. S4C) and upregulation of GAD1 (GAD67) (Fig. S4D) in islets from T2D donors compared to ND donors, supporting the notion that altered GABA shunt metabolism contributes to β cell dysfunction in T2D [41].

Given the changes in <code>gad1/gad2</code> expression and the crucial role of cytosolic GAD in converting glutamate to GABA, we also measured GAD enzyme activity. Interestingly, we found increased GAD activity in <code>Aass-KD</code> cells compared to NC cells (Fig. 5G). These findings suggests that the reduced GABA-to-glutamate ratio may not result from reduced GAD activity but instead from reduced substrate (i.e. glutamate) availability in the cytosol. Again, another hypothesis would be an accelerated GABA catabolism via GABA shunt, resulting in reducing GABA cell content.

Alternatively, the reduced intracellular GABA-to-glutamate ratio observed in Aass-KD cells might reflect altered secretion dynamics of these metabolites, rather than changes in their intracellular metabolic turnover. To address this, we examined the expression of subunits of the volume-regulated anion channel (VRAC), recently identified as the GABA efflux channel responsible for non-vesicular/cytosolic GABA release from β cells [42]. We observed altered expression of VRAC subunits, including Lrrc8d (the GABA-specific subunit) (Fig. S4E). However, the extracellular levels of glutamate and GABA mirrored the intracellular levels, with increased glutamate (Fig. S4F) and decreased GABA (Fig. S4G) concentrations, leading to a reduced GABA-toglutamate ratio in the extracellular medium of Aass-KD vs. NC cells (Fig. S4H). Thus, the observed differences in intracellular levels appear to stem from metabolic alterations rather than from changes in their secretory rates, supporting the role of AASS-dependent lysine catabolism in regulating glutamate and GABA metabolism.

Supporting a role for AASS-mediated lysine metabolism in GABA signaling, we found altered expression of several genes related to GABA signaling pathways, including genes encoding GABA receptor subunits (Fig. S4I), GABAergic transmission-related proteins (Fig. S4J), and adenylate cyclase subunits (Fig. S4K).

Therefore, we then investigated how inhibition of AASS-dependent lysine degradation affects glucose- and GABA-provoked calcium responses.

Consistent with the reduced GSIS, the glucose-stimulated cytosolic calcium oscillations in NC cells (Fig. 5H) were attenuated in Aass-KD cells (Fig. 5I-K). Acute GABA stimulation (10 μ M) enhanced the calcium response by approximately 14 % in NC cells (Fig. 5H, M). In Aass-KD cells, the GABA-induced calcium responses were diminished compared to controls (Fig. 5I, J, L). Notably, however, the relative increase in GABA-induced calcium response reached ~40 % in Aass-KD cells compared to ~14 % in NC cells (Fig. 5M).

These findings indicate that suppression of AASS-dependent lysine catabolism reduces both glucose- and GABA-induced calcium oscillations, consistent with the impaired GSIS observed in Aass-KD cells. However, the combination of lower extracellular GABA levels, altered expression of GABA-A receptor subunits, and the heightened relative calcium response to GABA in Aass-KD cells suggests a compensatory increase in their sensitivity to GABA signaling.

3.6. Exogenous GABA restores GSIS in Aass-KD cells

To further investigate the metabolic alterations underlying the reduced GABA/glutamate ratio and impaired GSIS in *Aass*-KD cells, we conducted a systematic functional analysis using pharmacological agents targeting key enzymes in the GABA shunt and GABA signaling pathway (see scheme in Fig. 6A). Specifically, we assessed the effects of allylglycine (GAD inhibitor), vigabatrin/ γ -vinyl GABA (GABA-T inhibitor), α -ketoisocaproic acid (α -KIC, GDH activator), leucine (allosteric activator of GDH) + glutamine (glutamate precursor, GDH substrate), muscimol (GABA-A receptor agonist), and GABA on insulin secretion.

Given the observed reduction in the GABA-to-glutamate ratio in *Aass*-KD cells, we initially hypothesized that impaired GABA synthesis,

specifically the conversion of glutamate to GABA via GAD, might underlie this alteration. As mentioned above, the change in expression of gad1/gad2 and increased GAD-specific activity in Aass-KD cells also suggest the participation of this pathway in the Aass-KD cells phenotype. Thus, to test this hypothesis, we inhibited GAD activity using allylglycine and measured GSIS in NC and Aass-KD cells (Fig. 6B). Interestingly and consistently with previous reports in human islets [42], GAD inhibition enhanced GSIS in NC cells (+115 %). This stimulatory effect was relatively more pronounced in Aass-KD cells (+151 %). However, despite this increase, GSIS in Aass-KD cells remained lower than in NC cells (Fig. 6B). These results indicate that inhibition of GABA synthesis, specifically by conversion of glutamate to GABA by GAD does not impair GSIS, in fact, it enhances it, thereby ruling out a reduced GABA synthesis by GAD as the primary cause of β -cell dysfunction in Aass-KD cells.

Next, to determine whether accelerated GABA catabolism might instead account for the reduced GABA-to-glutamate ratio and the associated functional impairments in Aass-KD cells, we focused on mitochondrial GABA transaminase (GABA-T), the enzyme responsible for converting GABA into succinic semialdehyde (SSA) and α -ketoglutarate (α -KG) into glutamate. Notably, as previously shown, expression of the gene encoding GABA-T, Abat, was downregulated in Aass-KD cells (Fig. 5F). Thus, to assess the potential contribution of an altered GABA-T activity to the observed phenotype, we inhibited GABA-T with vigabatrin and measured GSIS. Vigabatrin treatment did not significantly affect GSIS in either NC or Aass-KD cells (Fig. 6C), suggesting that accelerated GABA degradation via GABA-T is unlikely to underlie the reduced GABA/glutamate ratio and the impaired GSIS observed in Aass-KD cells.

Given the interplay between AASS-dependent lysine catabolism, the GABA shunt, and GDH activity in regulating glutamate and GABA metabolism (see schematic in Fig. 6A), and the pivotal role of GDHdriven anaplerosis in controlling GSIS [43], we examined whether altered GDH activity might underlie the impaired GSIS observed in Aass-KD cells. Activation of GDH with $\alpha\textsc{-KIC}$ significantly increased GSIS in NC cells (+103 %), whereas this increase was attenuated in Aass-KD cells (+84 %), potentially reflecting limited GDH substrate availability. As previously reported in rat islets, co-stimulation with leucine and glutamine in NC cells led to a robust increase in insulin secretion even at basal glucose levels, due to the synergistic effect of GDH activation and provision of anaplerotic substrates that fuel the TCA cycle, thereby enhancing mitochondrial ATP production independently of glucose [44]. Interestingly, in the presence of glucose, leucine plus glutamine elicited a greater relative increase in insulin secretion in Aass-KD cells (+67 %) than in NC cells (+51 %) (Fig. 6E). These findings, together with the reduced Glud1 mRNA (Fig. 5F) but unchanged GDH protein levels in Aass-KD cells (Fig. S4L-M), support the notion that reduced substrate availability, rather than decreased GDH abundance, may limit metabolic flux through GDH, thereby partially contributing to the blunted GSIS observed in Aass-KD cells.

Since GABA can act as an autocrine excitatory signal through GABA-A receptors to enhance insulin secretion in human β cells [45], we next investigated whether GABA-A receptor activation could rescue GSIS in Aass-KD cells. Indeed, muscimol treatment increased GSIS in NC cells (+57 %), with a slight pronounced effect in Aass-KD cells (+62 %) (Fig. 6F), consistent with the heightened relative GABA sensitivity in calcium responses observed in Aass-KD cells (Fig. 5M). However, GSIS remained lower in Aass-KD compared to NC cells, indicating that GABA-A receptor activation only partially restored insulin secretion.

Next, we tested whether direct GABA replenishment, which could both activate GABA-A receptors and as energy substrate to compensate for potential metabolic imbalances, could restore GSIS in *Aass*-KD cells. Notably, at 1 μ M GABA, GSIS was partially restored, while at 10 μ M GABA, GSIS was fully recovered (Fig. 6G). GABA replenishment also recovered GSIS in human islets from ND donors (Fig. 6H).

Finally, to explore the clinical relevance of these findings, we assessed the effects of acute GABA stimulation on GSIS in human islets from ND and T2D donors. In ND islets, GABA reduced basal insulin

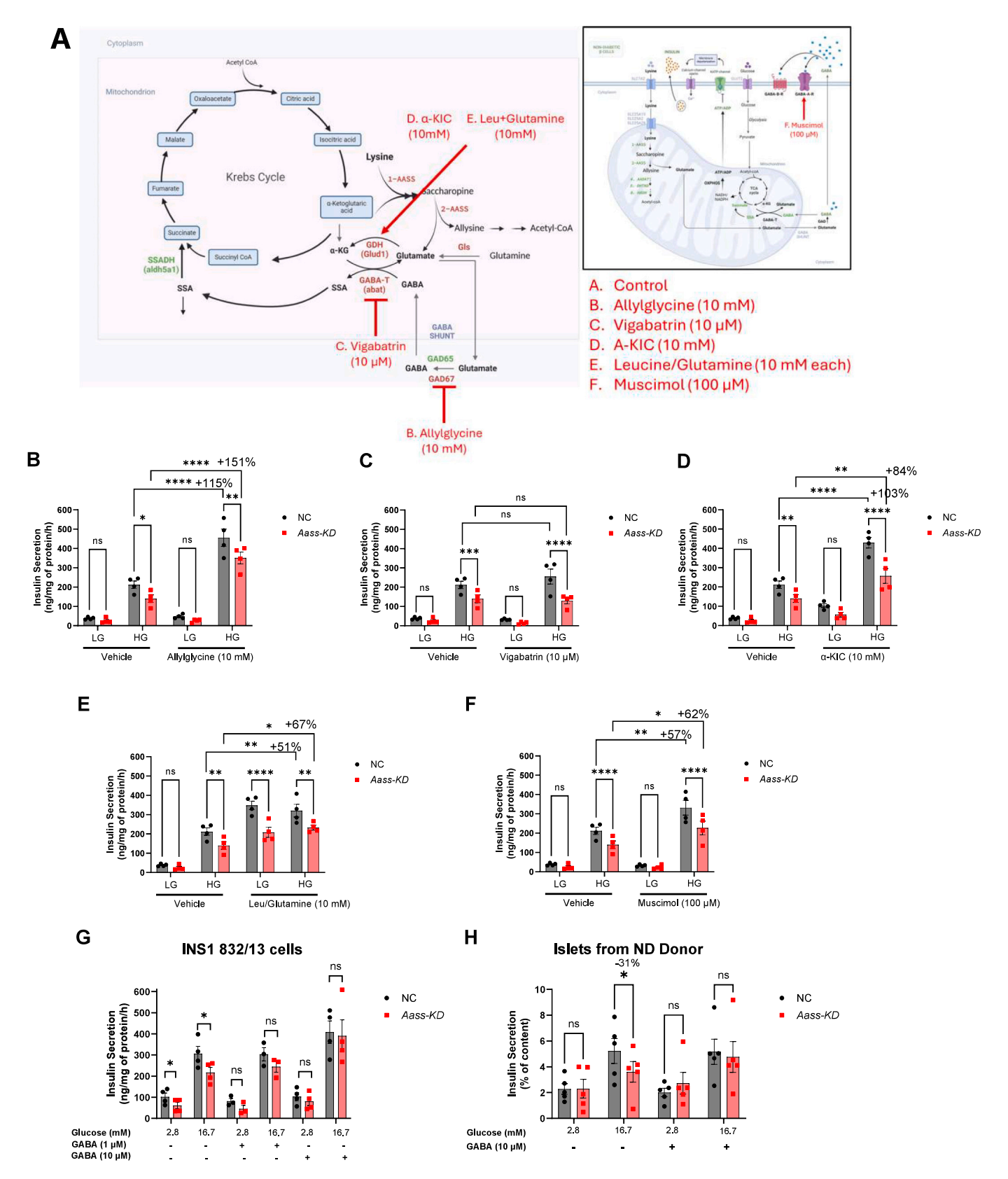


Fig. 6. Exogenous GABA Restores GSIS in *Aass*-KD Cells. **A.** Chart of interconnection of AASS-dependent lysine catabolism, TCA cycle, GDH anaplerosis, GABA shunt and GABA-A receptor pathways and specification of pharmacological agents used to manipulate these pathways. **B**—**H.** Effects on GSIS in NC and *Aass-KD* cells in response to acute (1 h) manipulation of above mentioned pathways by using the next pharmacological agents: **B.** allylglycine (GAD inhibitor), **C.** vigabatrin (γ-vinyl GABA, GABA-T inhibitor), **D.** α-ketoisocaproic acid (α-KIC, GDH activator), **E.** leucine (GDH activator) + glutamine (glutamate precursor), **F.** muscimol (GABA-A receptor agonist), and **G.** GABA (1 and 10 μM) (n = 4). **H.** Insulin secretion at LG and HG in the absence or presence of GABA (10 μM) in NC and *AASS-KD* ND islets (n = 5). All graphs show individual data points and mean \pm s.e.m. Statistical test: Two-way ANOVA (B—H). *p < 0.05, **p < 0.01, ***p < 0.001, ****p < 0.0001.

secretion (Fig. S4N) and increases the GSIS stimulatory index (Fig. S4O) and this effect was absent in T2D islets (Fig. S4P-Q).

3.7. Silencing of Aass results in altered mitochondrial TCA cycle and ATP production

Mitochondrial GABA and glutamate metabolism via the GABA shunt and GDH pathways plays a crucial role in GSIS by providing anaplerotic substrates to the TCA cycle in β cells [40,41,43]. In line with this, transcriptomic and metabolomic analyses of *Aass*-KD and NC INS1 832/13 cells also revealed alterations in the expression of genes and the abundance of metabolites related to glycolysis, TCA cycle and oxidative phosphorylation (OXPHOS) (Fig. 7).

We observed increased expression of Foxk1 and Ldhb in Aass-KD cells

(Fig. 7A). FOXK1, forkhead transcription factors 1, is activated during fasting and starvation to promote glycolysis while inhibiting mitochondrial pyruvate oxidation [46]. Consistently, *Aass*-KD cells showed decreased intracellular pyruvate levels and increased lactic acid compared to NC cells (Fig. 7B). These changes suggest impaired mitochondrial glucose metabolism in *Aass*-KD cells, with a shift of pyruvate from entering the TCA cycle to being converted into lactate. This idea is further supported by the elevated lactate-to-pyruvate ratio observed in *Aass*-KD cells in response to glucose (Fig. 7C), along with increased lactate secretion (Fig. 7D).

In support of reduced mitochondrial oxidation of pyruvate in *Aass*-KD cells, we also observed altered expression of genes encoding mitochondrial TCA cycle proteins (Fig. 7E, G) and reduced levels of key TCA cycle intermediates, including citric acid, succinic acid, and fumaric

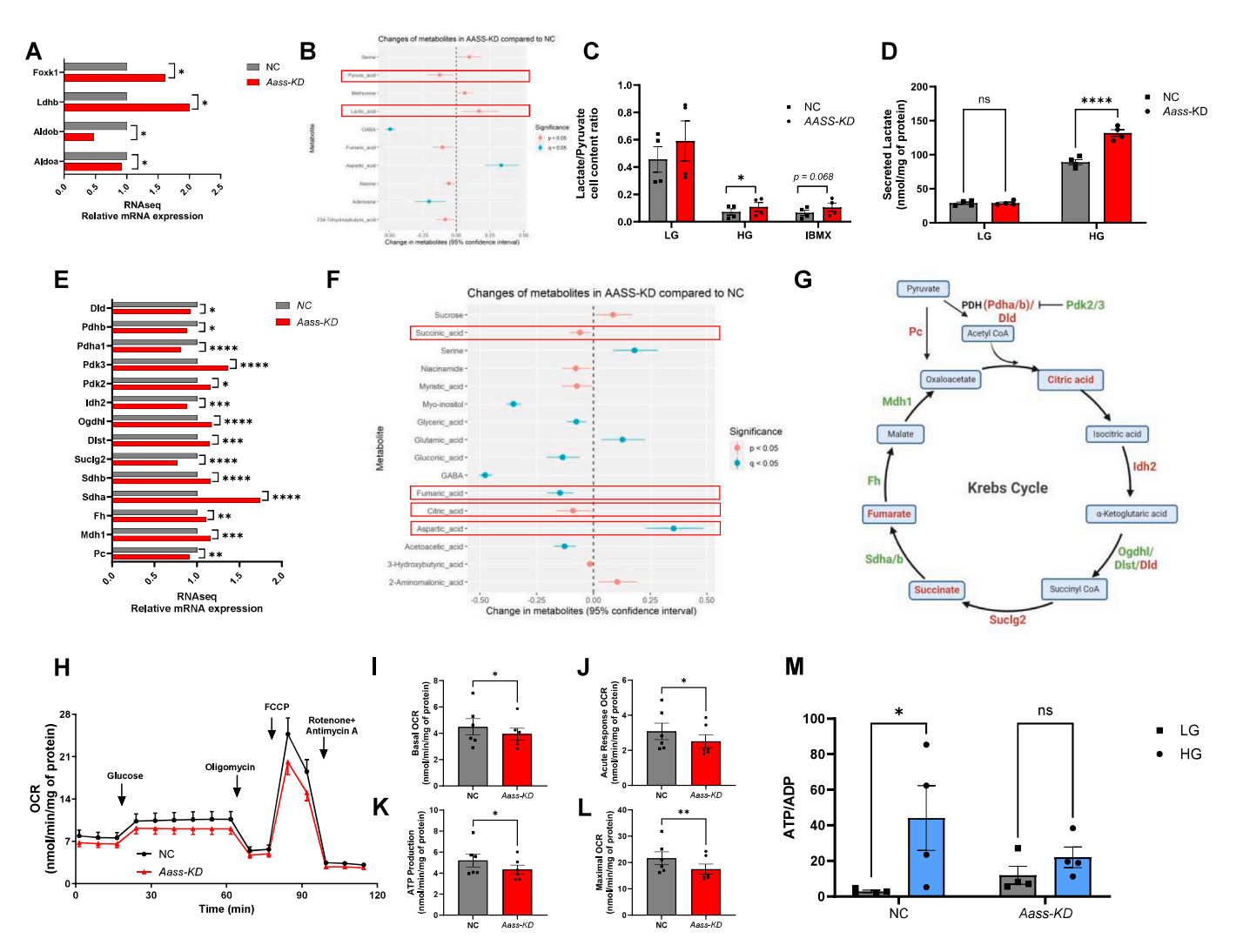


Fig. 7. Silencing of Aass Results in Altered Mitochondrial TCA Cycle and ATP production. **A.** Average expression levels of glycolysis-related genes in NC and Aass-KD INS1 832/13 β cells (n = 4). **B.** Plot showing differences in glycolysis-related metabolites cell contents in NC vs. Aass-KD INS1 832/13 β cells (n = 7). **C.** Lactate to pyruvate cell content ratio at LG, HG and HG + IBMX in NC control and Aass-KD INS1 832/13 β cells (n = 4). **D.** Lactate concentration in extracellular medium at LG and HG in NC control vs. Aass-KD INS1 832/13 β cells (n = 4). **E.** Average expression levels of TCA cycle-related genes in NC control and Aass-KD INS1 832/13 β cells (n = 4). **G.** Chart of TCA cycle pathway, highlighting DEGs and changes in metabolites cell contents in NC control INS1 832/13 β cells, in green upregulated genes, in red, down-regulated genes or less abundant metabolites. **H-L.** Mitochondrial OCR in NC and Aass-KD INS1 832/13 β cells (n = 6). **H.** Average OCR traces at LG, HG, Oligomycin (4 mM), FCCP (4 mM) and Antimycin A + Rotenone (1 mM) conditions. **I-L.** Comparison of calculated mitochondrial respiratory parameters in NC vs. Aass-KD INS1 832/13 β cells (n = 6); **I.** Basal OCR, **J.** Acute Response OCR, **K.** ATP-linked OCR, **L.** Maximal OCR. **M.** Whole-cell ATP to ADP content ratio measured by LC-MS after 60 min of stimulation with LG or HG in NC control vs. Aass-KD INS1 832/13 β cells (n = 4). All graphs show individual data points and mean ± s.e.m. Statistical tests: ANOVA (A, C-E, M), Student t-test (I-L). *p < 0.05, **p < 0.01, ***p < 0.001, ****p < 0.0001. KD, knockdown; NC, normal control; DEG, differentially expressed gene; LC-MS, liquid chromatography-mass spectrometry; OCR, oxygen consumption rate. (For interpretation of the references to colour in this figure legend, the reader is referred to the web version of this article.)

acid, alongside increased aspartic acid levels (Fig. 7F, G).

The ketone bodies; acetoacetate and 3-hydroxybutyrate serve to anaplerotically feed the TCA cycle and in combination with other substrates stimulates insulin secretion [47]. Coenzyme A conjugated forms of these metabolites are produced along the lysine catabolic pathway (Fig. 4D) and they were also reduced in *Aass*-KD compared to NC cells (Fig. 7F).

To further assess how these TCA cycle alterations in Aass-KD cells might affect mitochondrial OXPHOS, we measured oxygen consumption rate (OCR) in response to glucose and mitochondrial inhibitors, which allowed us to calculate key respiratory parameters (Fig. 7H-L). The analysis revealed significantly reduced mitochondrial respiration in Aass-KD cells compared to NC cells. This included reductions in basal OCR (Fig. 7I), acute response OCR (Fig. 7J), ATP-linked OCR (Fig. 7K), and maximal OCR (Fig. 7L). These findings are consistent with a blunted increase in the ATP/ADP cell content ratio in Aass-KD cells following glucose stimulation, whereas control NC cells showed an expected rise (Fig. 7M). These overall reduced TCA cycle and OXPHOS activity in response to suppressing lysine catabolism in Aass-KD cells was also aligned with altered expression of multiple genes encoding subunits of Complex I (Fig. S5A), II (Fig. S5B), III (Fig. S5C), IV (Fig. S5D) and V (Fig. S5E) of OXPHOS.

Together, these results indicate that suppression of AASS-dependent lysine metabolism in β cells may limit glutamate availability for GDH-mediated anaplerosis of the TCA cycle and disrupt GABA-related metabolism and signaling. Consequently, mitochondrial OXPHOS is impaired and the ATP/ADP ratio reduced, contributing to defective GSIS.

4. Discussion

Lysine is an essential amino acid with insulinotropic effects in humans and in β -cell models [2–4,48,49]. Here, we investigated whether this action requires AASS-dependent lysine catabolism. Our findings indicate that AASS-dependent lysine catabolism supports GDH-mediated anaplerosis and GABA cell content, sustaining mitochondrial

function and potentiating insulin secretion. Accordingly, reduced AASS-dependent lysine catabolism activity, as observed in islets from individuals with T2D, may contribute to GABA depletion, altered GABAergic signaling, reduced GDH-mediated anaplerosis, impaired mitochondrial ATP production, and β -cell dysfunction (Fig. 8).

For decades, the insulinotropic effect of lysine was attributed to membrane depolarization (by analogy to arginine) [4]. In this study, we demonstrated that human islets and INS1 832/13 β cells express enzymes of the lysine catabolic pathway, and that silencing AASS, its ratelimiting enzyme, diminishes both lysine-promoted GSIS and GSIS. Therefore, the insulinotropic effect observed following intravenous lysine administration in humans [2], as well as in isolated β cells and rodent islets [4,48,49], is likely attributable, at least in part, to AASS-dependent lysine catabolism within β cells. Our data further indicate that glucose engages AASS-dependent lysine catabolism to potentiate GSIS, consistent with prior metabolomic evidence showing that glucose enhances lysine catabolism in β cells in parallel with insulin secretion [59,60].

Mechanistically, our results support a model in which AASS-derived glutamate supplies GDH to fuel TCA-cycle anaplerosis [42,63]. Consistent with this, α -KIC activation of GDH produced a smaller GSIS increase in Aass-KD cells, while leucine (GDH activator) plus glutamine (glutamate precursor) produced a relatively greater increases of insulin secretion in Aass-KD than in control cells. Transcriptomic and metabolomic data align with impaired anaplerosis, indicating reduced TCAcycle activity, defective OXPHOS, a shift from mitochondrial pyruvate oxidation toward lactate synthesis, reduced oxygen consumption rate, and a decreased ATP/ADP ratio. Because ATP-sensitive K+-channel closure is required for depolarization and Ca²⁺ influx [50-52], these molecular defects mechanistically explain the blunted GSIS. In addition, lysine catabolism-derived acetoacetate and 3-hydroxybutyrate [53-55], ketone bodies that serve as alternative anaplerotic substrates and support GSIS in β cells [47], were markedly reduced following AASS silencing. This suggests that the loss of lysine-derived ketone anaplerosis may further limit TCA cycle flux. Together, these findings indicate an imbalance between anaplerosis and cataplerosis, leading to limited

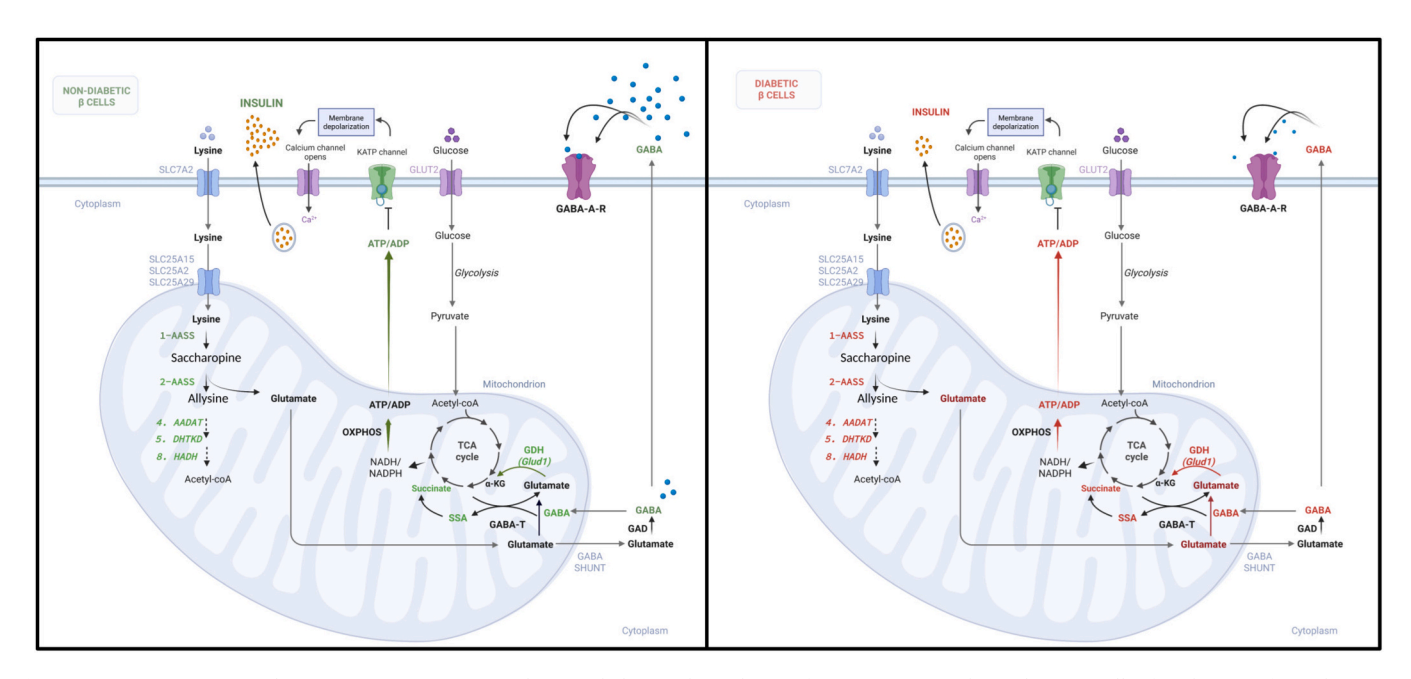


Fig. 8. Lysine Potentiates Insulin Secretion via AASS-Dependent Catabolism and Regulation of GABA Content and Signaling in β cells of ND but not of T2D donors. In β cells from non-diabetic (ND) donors, lysine potentiates insulin secretion through its AASS-dependent catabolism. This metabolic pathway provides glutamate, which serves as a substrate for both GABA shunt metabolism and anaplerotic entry into the TCA cycle via GDH, enhancing mitochondrial ATP production and, consequently, insulin secretion. In contrast, in β cells from type 2 diabetes (T2D) donors, the reduced expression of genes involved in lysine catabolism, including AASS, leads to suppressed lysine metabolism. This results in decreased GABA cell content, impaired GABA-A receptor signaling, and diminished anaplerotic fuelling of the TCA cycle through the GDH pathway. Consequently, mitochondrial ATP production and insulin secretion are reduced.

availability of TCA cycle intermediates and an uncoupling of cytosolic glycolysis from mitochondrial oxidation. This is supported by the accumulation of lactate and aspartate, along with reduced succinate and fumarate, consistent with impaired malate-aspartate shuttle activity and insufficient NAD⁺ regeneration in the cytosol [56,57].

At the level of GABA homeostasis, suppression of AASS-dependent lysine catabolism reduced β cell GABA content and altered the GABA/ glutamate ratio. This mirrors prior observations that mitochondrial stress associates with lower intracellular GABA (e.g., MIRO1/RHOT1 silencing reduces GABA content, mitochondrial respiration and GSIS) [58]. Functionally, exogenous GABA restored GSIS in both β cells and human islets with AASS silencing, implicating reduced GABA availability as a causal contributor to secretory failure. Pharmacology further refined mechanism: GABA-T inhibition (vigabatrin) did not improve GSIS, whereas GAD inhibition (allylglycine) enhanced GSIS in control cells and produced an even greater relative increase in Aass-KD cells, yet GSIS in Aass-KD cells remained lower than in control cells. Thus, reduced GABA synthesis via GAD is unlikely the primary defect; rather, limited glutamate supply, altered mitochondrial flux through GDH, and disrupted GABA turnover that collectively results in GABA depletion and impaired GSIS.

At the signaling level, Aass-KD cells displayed attenuated glucoseevoked Ca²⁺ oscillations and reduced GABA-evoked Ca²⁺ responses, yet a relatively greater sensitivity to GABA, alongside an altered expression of the GABA-A receptor subunits, consistent with compensatory receptor hypersensitivity in the setting of low extracellular GABA [13]. In ND human islets, acute stimulation with GABA lowered basal insulin secretion and thereby increased the stimulatory index of GSIS, indicating a glucose-dependent, modulatory action, likely via GABA-A receptors. This effect was, however, absent in T2D islets, consistent with loss of GABA responsiveness. By contrast, exogenous GABA restored GSIS in both β cells and ND human islets with silencing of AASS, suggesting that under AASS deficiency, the metabolic (substrate) contribution of GABA can dominate over autocrine signaling to rescue mitochondrial support of secretion. Importantly, this interpretation is supported by prior electrophysiological evidence from Korol et al. [13], who demonstrated that maximal activation of native β cell GABA-A receptors occurs at nanomolar concentrations (100-1000 nM), with saturation at micromolar levels. Given that GSIS rescue in our experiments required 10 µM GABA, it is unlikely that receptor-mediated signaling accounts for such recovery effect, and more plausible that GABA acted as a metabolic anaplerotic substrate to replenish mitochondrial intermediates and restore secretory competence.

The role of GABA in GSIS, whether stimulatory or inhibitory, and whether mediated via the GABA shunt, autocrine signaling, or both, remains debated. Pizarro-Delgado et al. [40] reported that glucose promotes GABA shunt activity to support insulin secretion, as inhibition of GABA transaminase reduced GSIS in rat islets. In contrast, Menegaz et al. [42] emphasized cytosolic GABA for autocrine signaling, showing that human β cells release GABA in a pulsatile manner to synchronize insulin secretion, and that elevating intracellular GABA by blocking GABA-T resulted in reduced insulin secretion. Similarly, GAD inhibition lowered GABA content and pulsatile release, enhancing GSIS in human islets, consistent with evidence that GABA-A receptor activation can suppress exocytosis [13]. Conversely, Braun et al. [45] reported GABA acting as an excitatory autocrine signal via GABA-A receptors to enhance secretion. Our data in human islets from ND donors show that GABA suppressed insulin secretion at low glucose yet increased the stimulatory index of GSIS, underscoring its glucose-dependent actions. As with other neurotransmitters involved in β -cell regulation, such as serotonin [59–61], the effects of GABA on GSIS likely reflect an integrated balance between its intracellular metabolism [41], as a mitochondrial anaplerotic substrate and precursor of glutamate, and its extracellular receptormediated signaling [42,45], an interplay that is highly context- and condition-dependent.

Our comparative transcriptomic and proteomic analyses of

pancreatic islets from T2D versus ND donors reveal a reduction in AASS expression, along with downregulation of additional components of the lysine catabolic pathway. These alterations are accompanied by dysregulated expression of GABA-pathway–related genes, including GAD1, GABRA1, and GABRA2 [33]. Notably, T2D islets exhibit both GABA depletion [13,42,62,63] and supersensitive GABA-A receptor responses [13]. Our data suggest that suppressed AASS-dependent lysine catabolism may represent a common upstream mechanism linking reduced GABA availability with compensatory GABA-A receptor hypersensitivity, thereby impairing β cell communication and GSIS in both experimental AASS deficiency and T2D.

Extending beyond the pancreas, defects in lysine catabolism are clinically relevant in the central nervous system. Pyridoxine-dependent epilepsy (PDE; OMIM 266100) [64] is caused by mutations in ALDH7A1, which encodes the enzyme catalysing the reaction immediately downstream of AASS. These mutations lead to the accumulation of α -aminoadipate semialdehyde, depletion of pyridoxal-5-phosphate (PLP), and consequent reduction of PLP-dependent GAD activity, resulting in diminished GABA production in patient fibroblasts [65]. Thus, disruption of lysine catabolism pathway at either, AASS or ALDH7A1 reactions, seems to converge on cellular GABA depletion. These parallels underscore the nutritional importance of maintaining adequate dietary intake of this essential amino acid and highlight the central role of AASSdependent lysine catabolism in sustaining GABA/glutamate homeostasis. They further suggest that therapeutic inhibition of AASS, such as that proposed for pyridoxine-dependent epilepsy (PDE) [66], should be carefully evaluated for potential adverse effects on pancreatic islet function and glycemic control.

Our findings raise the possibility that the neurocognitive impairment observed in patients with hyperlysinemia caused by AASS mutations may result, at least in part, from disrupted AASS-dependent lysine catabolism, leading to altered GABA/glutamate homeostasis and signaling, as well as impaired GDH-dependent mitochondrial anaplerosis within the central nervous system. Given that these neurotransmitter pathways are essential for neuronal communication, synaptic plasticity, and brain development, their dysregulation provides a plausible mechanistic link between AASS-related metabolic dysfunction and the neurodevelopmental deficits associated with hyperlysinemia.

While our study provides comprehensive mechanistic insights into the role of AASS-dependent lysine catabolism in β cell function, some limitations should be acknowledged. First, our findings rely primarily on in vitro and ex vivo models, and the effects of β cell-specific AASS silencing in vivo remain untested. Thus, the impact of impaired β cells lysine catabolism on systemic glucose homeostasis is still unknown. Second, the lysine concentrations we used (10 mM) exceed fasting (\sim 0.1–0.3 mM) and postprandial (\sim 0.2–0.6 mM) plasma levels, although total circulating amino acid pools can reach 2-5 mM [67-69]. In addition, pathological conditions such as hyperlysinemia can also elevate plasma lysine to ~2 mM [70]. Our dose-response experiments (data not shown) showed a trend toward increased GSIS at 1 mM and a significant effect at 5 mM lysine, supporting the physiological relevance of our findings. Moreover, previous studies have supported the use of such elevated lysine concentrations in vitro in order to mimic the synergistic action of amino acid pools in vivo [71]. Third, discrepancies among models, such as the divergent IBMX responses in INS1 cells versus human islets, underscore the influence of intra-islet paracrine interactions not captured in clonal β cell lines. Fourth, although transcriptomic, metabolomic, and pharmacological analyses point to disrupted GABA/glutamate metabolism and reduced GDH-mediated anaplerosis downstream of AASS deficiency, direct metabolic flux measurements are needed to validate these pathways. Finally, while GABA supplementation restored GSIS, intracellular GABA levels and shunt activity were not quantified in human AASS-KD islets due to limited material, representing a key area for future study. Addressing these gaps, particularly via β cell-specific Aass-KO in vivo models and metabolic flux analyses, will be essential to fully elucidate how lysine

catabolism supports $\boldsymbol{\beta}$ cell metabolic integrity, insulin secretion and glucose homeostasis.

5. Conclusion

AASS-dependent lysine catabolism emerges as a key regulator of β -cell function, sustaining GDH-driven anaplerosis, GABA homeostasis, and mitochondrial metabolism. Its suppression reduces GABA content, limits anaplerotic flux, disrupts OXPHOS, dampens Ca^{2+} oscillations, and impairs GSIS. The reduction of lysine-catabolic gene expression in T2D islets suggests a mechanistic link to β -cell GABA depletion and mitochondrial failure. Restoration of GSIS by exogenous GABA in AASS-deficient β cells and human islets highlights the dual metabolic and signaling roles of GABA in supporting secretion. These findings also underscore the nutritional importance of essential amino acids, such as lysine, in regulating GSIS and systemic glucose homeostasis. Therapeutically, approaches that restore lysine catabolism and/or augment GABA content or signaling warrant evaluation for preserving β -cell function and glucose homeostasis.

CRediT authorship contribution statement

Felipe Munoz: Methodology, Investigation, Formal analysis. Qian Gao: Formal analysis, Data curation. Matthias Mattanovich: Methodology, Formal analysis. Kajetan Trost: Methodology, Formal analysis. Ondřej Hodek: Methodology, Formal analysis. Andreas Lindqvist: Methodology. Nils Wierup: Resources. Malin Fex: Writing – review & editing, Resources. Thomas Moritz: Writing – review & editing, Supervision, Resources, Funding acquisition. Hindrik Mulder: Writing – review & editing, Supervision, Resources, Funding acquisition. Luis Rodrigo Cataldo: Writing – review & editing, Writing – original draft, Visualization, Validation, Supervision, Resources, Project administration, Methodology, Investigation, Funding acquisition, Formal analysis, Data curation, Conceptualization.

Authorship contributions

L.R.C. conceptualized and designed the study. F.M, L.R.C., Q.G., M. M., K.T., A.L. performed experiments and analyzed data. Q.G., T.M, L.R. C., F.M performed statistical data analyses and assisted in experimental design. L.R.C., H.M., M.F., T.M. contributed to interpretation of data. L. R.C. wrote the manuscript. All authors revised the manuscript and approved the final version to be published. L.R.C. is the guarantor of this work and, as such, had full access to all the data in the study and takes responsibility for the integrity of the data and the accuracy of the data analysis.

Declaration of Generative AI and AI-assisted technologies in the writing process

During the preparation of this work the author(s) used ChatGPT (OpenAI, 2025), which was used to improve phrasing and clarity. After using this tool/service, the author(s) reviewed and edited the content as needed and take(s) full responsibility for the content of the publication.

Funding

This work was supported by the Novo Nordisk Foundation (NNF18CC0034900; NNF23SA0084103 unconditional donation to Novo Nordisk Foundation Center for Basic Metabolic Research) (T.M.), EFSD/Novo Nordisk A/S Programme for Diabetes Research in Europe 2023 (L.R.C.), The Albert Påhlsson Foundation 2024 (L.R.C.), The Royal Physiographic Society of Lund 2024 (L.R.C.), Bo & Kerstin Hjelt Diabetes Foundation (L.R.C.), The Crafoord Foundation (Reference Number: 20250592) (L.R.C.), The Novo Nordisk Leif Groop Young-Scientist Scholarship (L.R.C.), Swedish Foundation for Strategic Research

(LUDC-IRC; grant agreement number IRC15–0067), The Swedish Research Council, Strategic Research Area Exodiab (grant agreement number 2009–1039), The Swedish Research Council (2021–01116 to M. F.), The Novo Nordisk Foundation NNF23OC0084475 (M.F.), The Albert Påhlsson's Foundation (M.F.), Swedish Research Council (2021–01777) (H.M.), The Novo Nordisk Foundation (NNF23OC0084463) (H.M.).

Prior presentation

Preliminary results of this study were presented at the 58th and 60th Annual Meeting of the EASD, 2022 and 2024, respectively.

Declaration of competing interest

The authors declare that they have no known competing financial interests or personal relationships that could have appeared to influence the work reported in this paper.

Acknowledgements

We thank the Human Tissue Laboratory within EXODIAB/Lund University Diabetes Center. This work includes data and/or analyses from HumanIslets.com funded by the Canadian Institutes of Health Research, JDRF Canada, and Diabetes Canada (5-SRA-2021-1149-S-B/TG 179092) with data from islets isolated by the Alberta Diabetes Institute IsletCore with the support of the Human Organ Procurement and Exchange program, Trillium Gift of Life Network, BC Transplant, Quebec Transplant, and other Canadian organ procurement organizations with written informed donor consent as approved by the Human Research Ethics Board at the University of Alberta (Pro00013094).

We would like to express our gratitude to Professor Patrick Macdonald from the University of Alberta and Jelena Kolic from the University of British Columbia, Canada, for their valuable assistance in clarifying aspects related to the data from humanislets.com. We also thank Anna-Maria Veljanovska Ramsay and Laila Jacobsson from Lund University for their technical support.

We acknowledge Christian Grønbæk and The Single-Cell Omics platform at the Novo Nordisk Foundation Center for Basic Metabolic Research (CBMR) for technical and computational expertise.

Appendix A. Supplementary data

Supplementary data to this article can be found online at $\frac{\text{https:}}{\text{doi.}}$ org/10.1016/j.metabol.2025.156423.

References

- Kolic J, et al. Proteomic predictors of individualized nutrient-specific insulin secretion in health and disease. Cell Metab 2024;36:1619–33. e1615, https://doi. org/10.1016/j.cmet.2024.06.001.
- [2] Floyd Jr JC, Fajans SS, Conn JW, Knopf RF, Rull J. Stimulation of insulin secretion by amino acids. J Clin Invest 1966;45:1487–502. https://doi.org/10.1172/ JCI105456.
- [3] Nilsson M, Stenberg M, Frid AH, Holst JJ, Bjorck IM. Glycemia and insulinemia in healthy subjects after lactose-equivalent meals of milk and other food proteins: the role of plasma amino acids and incretins. Am J Clin Nutr 2004;80:1246–53. https://doi.org/10.1093/ajcn/80.5.1246.
- [4] Liu Z, Jeppesen PB, Gregersen S, Chen X, Hermansen K. Dose- and glucose-dependent effects of amino acids on insulin secretion from isolated mouse islets and clonal INS-1E Beta-cells. Rev Diabet Stud 2008;5:232–44. https://doi.org/10.1900/RDS.2008.5.232.
- [5] Newsholme P, Bender K, Kiely A, Brennan L. Amino acid metabolism, insulin secretion and diabetes. Biochem Soc Trans 2007;35:1180–6. https://doi.org/ 10.1042/BST0351180.
- [6] Kolic J, Sun WG, Johnson JD, Guess N. Amino acid-stimulated insulin secretion: a path forward in type 2 diabetes. Amino Acids 2023;55:1857–66. https://doi.org/ 10.1007/s00726-023-03352-8.
- [7] Papes F, Surpili MJ, Langone F, Trigo JR, Arruda P. The essential amino acid lysine acts as precursor of glutamate in the mammalian central nervous system. FEBS Lett 2001;488:34–8. https://doi.org/10.1016/s0014-5793(00)02401-7.

- [8] Markovitz PJ, Chuang DT. The bifunctional aminoadipic semialdehyde synthase in lysine degradation. Separation of reductase and dehydrogenase domains by limited proteolysis and column chromatography. J Biol Chem 1987;262:9353–8.
- [9] Maechler P, Wollheim CB. Mitochondrial glutamate acts as a messenger in glucoseinduced insulin exocytosis. Nature 1999;402:685–9. https://doi.org/10.1038/ 45280
- [10] Prentki M, Matschinsky FM, Madiraju SR. Metabolic signaling in fuel-induced insulin secretion. Cell Metab 2013;18:162–85. https://doi.org/10.1016/j. cmet 2013 05 018
- [11] Gheni G, et al. Glutamate acts as a key signal linking glucose metabolism to incretin/cAMP action to amplify insulin secretion. Cell Rep 2014;9:661–73. https://doi.org/10.1016/j.celrep.2014.09.030.
- [12] Baekkeskov S, et al. Identification of the 64K autoantigen in insulin-dependent diabetes as the GABA-synthesizing enzyme glutamic acid decarboxylase. Nature 1990;347:151–6. https://doi.org/10.1038/347151a0.
- [13] Korol SV, et al. Functional characterization of native, high-affinity GABA(a) receptors in human pancreatic beta cells. EBioMedicine 2018;30:273–82. https://doi.org/10.1016/j.ebiom.2018.03.014.
- [14] Hagan DW, Ferreira SM, Santos GJ, Phelps EA. The role of GABA in islet function. Front Endocrinol (Lausanne) 2022;13:972115. https://doi.org/10.3389/fendo.2022.972115.
- [15] Razquin C, et al. Lysine pathway metabolites and the risk of type 2 diabetes and cardiovascular disease in the PREDIMED study: results from two case-cohort studies. Cardiovasc Diabetol 2019;18:151. https://doi.org/10.1186/s12933-019-0058-2
- [16] Wang TJ, et al. 2-Aminoadipic acid is a biomarker for diabetes risk. J Clin Invest 2013;123:4309–17. https://doi.org/10.1172/JCI64801.
- [17] Leandro J, Houten SM. The lysine degradation pathway: subcellular compartmentalization and enzyme deficiencies. Mol Genet Metab 2020;131:14–22. https://doi.org/10.1016/j.ymgme.2020.07.010.
- [18] Sacksteder KA, et al. Identification of the alpha-aminoadipic semialdehyde synthase gene, which is defective in familial hyperlysinemia. Am J Hum Genet 2000;66:1736–43. https://doi.org/10.1086/302919.
- [19] Asplund O, et al. Islet gene view-a tool to facilitate islet research. Life Sci Alliance 2022;5. https://doi.org/10.26508/lsa.202201376.
- [20] Hohmeier HE, et al. Isolation of INS-1-derived cell lines with robust ATP-sensitive K+ channel-dependent and -independent glucose-stimulated insulin secretion. Diabetes 2000;49:424–30.
- [21] Ravassard P, et al. A genetically engineered human pancreatic beta cell line exhibiting glucose-inducible insulin secretion. J Clin Invest 2011;121:3589–97. https://doi.org/10.1172/JCI58447.
- [22] Taneera J, et al. Identification of novel genes for glucose metabolism based upon expression pattern in human islets and effect on insulin secretion and glycemia. Hum Mol Genet 2015;24:1945–55. https://doi.org/10.1093/hmg/ddu610.
- [23] Wierup N, Svensson H, Mulder H, Sundler F. The ghrelin cell: a novel developmentally regulated islet cell in the human pancreas. Regul Pept 2002;107: 63–9. https://doi.org/10.1016/s0167-0115(02)00067-8.
- [24] Sato S, et al. Atlas of exercise metabolism reveals time-dependent signatures of metabolic homeostasis. Cell Metab 2022;34:329–45. e328, https://doi.org/10.10 16/j.cmet.2021.12.016.
- [25] Cataldo LR, et al. The human batokine EPDR1 regulates beta-cell metabolism and function. Mol Metab 2022;66:101629. https://doi.org/10.1016/j. molmet 2022 101629
- [26] Ewels PA, et al. The nf-core framework for community-curated bioinformatics pipelines. Nat Biotechnol 2020;38:276–8. https://doi.org/10.1038/s41587-020-0430-x
- [27] Frankish A, et al. GENCODE reference annotation for the human and mouse genomes. Nucleic Acids Res 2019;47:D766–73. https://doi.org/10.1093/nar/
- [28] Robinson MD, McCarthy DJ, Smyth GK. edgeR: a Bioconductor package for differential expression analysis of digital gene expression data. Bioinformatics 2010;26:139–40. https://doi.org/10.1093/bioinformatics/btp616.
- [29] The Gene Ontology, C. The gene Ontology resource: 20 years and still GOing strong. Nucleic Acids Res 2019;47:D330–8. https://doi.org/10.1093/nar/ gkv1055
- [30] Fabregat A, et al. The Reactome pathway knowledgebase. Nucleic Acids Res 2018; 46:D649–55. https://doi.org/10.1093/nar/gkx1132.
- [31] Wu D, Smyth GK. Camera: a competitive gene set test accounting for inter-gene correlation. Nucleic Acids Res 2012;40:e133. https://doi.org/10.1093/nar/ gks461
- [32] Johnson WE, Li C, Rabinovic A. Adjusting batch effects in microarray expression data using empirical Bayes methods. Biostatistics 2007;8:118–27. https://doi.org/ 10.1093/biostatistics/kxi037.
- [33] Bacos K, et al. Type 2 diabetes candidate genes, including PAX5, cause impaired insulin secretion in human pancreatic islets. J Clin Invest 2023;133. https://doi. pp. 10.1179/JCM162619
- [34] Lawlor N, et al. Multiomic profiling identifies cis-regulatory networks underlying human pancreatic beta cell identity and function. Cell Rep 2019;26:788–801. e786, https://doi.org/10.1016/j.celrep.2018.12.083.
- [35] Drucker DJ. The biology of incretin hormones. Cell Metab 2006;3:153–65. https://doi.org/10.1016/j.cmet.2006.01.004.
- [36] Cataldo LR, et al. The MafA-target gene PPP1R1A regulates GLP1R-mediated amplification of glucose-stimulated insulin secretion in beta-cells. Metabolism 2021;118:154734. https://doi.org/10.1016/j.metabol.2021.154734.

- [37] Rorsman P, Huising MO. The somatostatin-secreting pancreatic delta-cell in health and disease. Nat Rev Endocrinol 2018;14:404–14. https://doi.org/10.1038/ s41574-018-0020-6.
- [38] Gheibi S, et al. Reduced expression level of protein phosphatase PPM1E serves to maintain insulin secretion in type 2 diabetes. Diabetes 2023;72:455–66. https://doi.org/10.2337/db22-0472.
- [39] Karaca M, Frigerio F, Maechler P. From pancreatic islets to central nervous system, the importance of glutamate dehydrogenase for the control of energy homeostasis. Neurochem Int 2011;59:510–7. https://doi.org/10.1016/j.neuint.2011.03.024.
- [40] Pizarro-Delgado J, Braun M, Hernandez-Fisac I, Martin-Del-Rio R, Tamarit-Rodriguez J. Glucose promotion of GABA metabolism contributes to the stimulation of insulin secretion in beta-cells. Biochem J 2010;431:381–9. https://doi.org/10.1042/BJ20100714.
- [41] Tamarit-Rodriguez J. Metabolic role of GABA in the secretory function of pancreatic beta-cells: its hypothetical implication in beta-cell degradation in type 2 diabetes. Metabolites 2023;13. https://doi.org/10.3390/metabo13060697.
- [42] Menegaz D, et al. Mechanism and effects of pulsatile GABA secretion from cytosolic pools in the human beta cell. Nat Metab 2019;1:1110–26. https://doi.org/ 10.1038/s42255-019-0135-7.
- [43] Gheibi S, et al. Conversion of glutamate into proline by the leucine analog BCH enhances biphasic insulin secretion in pancreatic beta-cells. J Biol Chem 2025; 108449. https://doi.org/10.1016/j.jbc.2025.108449.
- [44] Sener A, Somers G, Devis G, Malaisse WJ. The stimulus-secretion coupling of amino acid-induced insulin release. Biosynthetic and secretory responses of rat pancreatic islet to L-leucine and L-glutamine. Diabetologia 1981;21:135–42. https://doi.org/ 10.1007/BF00251281.
- [45] Braun M, et al. Gamma-aminobutyric acid (GABA) is an autocrine excitatory transmitter in human pancreatic beta-cells. Diabetes 2010;59:1694–701. https://doi.org/10.2337/db09-0797.
- [46] Sukonina V, et al. FOXK1 and FOXK2 regulate aerobic glycolysis. Nature 2019;566: 279–83. https://doi.org/10.1038/s41586-019-0900-5.
- [47] MacDonald MJ, et al. Acetoacetate and beta-hydroxybutyrate in combination with other metabolites release insulin from INS-1 cells and provide clues about pathways in insulin secretion. Am J Phys Cell Phys 2008;294:C442–50. https://doi. org/10.1152/aipcell.00368.2007.
- [48] McClenaghan NH, Barnett CR, O'Harte FP, Flatt PR. Mechanisms of amino acidinduced insulin secretion from the glucose-responsive BRIN-BD11 pancreatic B-cell line. J Endocrinol 1996;151:349–57. https://doi.org/10.1677/joe.0.1510349.
- [49] Sener A, et al. Stimulus-secretion coupling of arginine-induced insulin release: comparison with lysine-induced insulin secretion. Endocrinology 1989;124: 2558–67. https://doi.org/10.1210/endo-124-5-2558.
- [50] Ashcroft FM, Harrison DE, Ashcroft SJ. Glucose induces closure of single potassium channels in isolated rat pancreatic beta-cells. Nature 1984;312:446–8. https://doi. org/10.1038/312446a0.
- [51] Munoz F, Fex M, Moritz T, Mulder H, Cataldo LR. Unique features of beta-cell metabolism are lost in type 2 diabetes. Acta Physiol (Oxford) 2024;240:e14148. https://doi.org/10.1111/apha.14148.
- [52] Cook DL, Hales CN. Intracellular ATP directly blocks K+ channels in pancreatic Bcells. Nature 1984:311:271–3.
- [53] Papes F, Kemper EL, Cord-Neto G, Langone F, Arruda P. Lysine degradation through the saccharopine pathway in mammals: involvement of both bifunctional and monofunctional lysine-degrading enzymes in mouse. Biochem J 1999;344(Pt 2):555-63
- [54] Markovitz PJ, Chuang DT, Cox RP. Familial hyperlysinemias. Purification and characterization of the bifunctional aminoadipic semialdehyde synthase with lysine-ketoglutarate reductase and saccharopine dehydrogenase activities. J Biol Chem 1984;259:11643–6.
- [55] Rao VV, Pan X, Chang YF. Developmental changes of L-lysine-ketoglutarate reductase in rat brain and liver. Comp Biochem Physiol B 1992;103:221–4. https://doi.org/10.1016/0305-0491(92)90435-t.
- [56] Jitrapakdee S, Wutthisathapornchai A, Wallace JC, MacDonald MJ. Regulation of insulin secretion: role of mitochondrial signalling. Diabetologia 2010;53:1019–32. https://doi.org/10.1007/s00125-010-1685-0.
- [57] Eto K, et al. Role of NADH shuttle system in glucose-induced activation of mitochondrial metabolism and insulin secretion. Science 1999;283:981–5. https://doi.org/10.1126/science.283.5404.981.
- [58] Ronn T, et al. Genes with epigenetic alterations in human pancreatic islets impact mitochondrial function, insulin secretion, and type 2 diabetes. Nat Commun 2023; 14:8040. https://doi.org/10.1038/s41467-023-43719-9.
- [59] Cataldo LR, Cortes VA, Galgani JE, Olmos PR, Santos JL. Role of peripheral serotonin in the insulin secretion and glucose homeostasis. Nutr Hosp 2014;30: 498–508. https://doi.org/10.3305/nh.2014.30.3.7531.
- [60] Cataldo Bascunan LR, Lyons C, Bennet H, Artner I, Fex M. Serotonergic regulation of insulin secretion. Acta Physiol (Oxford) 2019;225:e13101. https://doi.org/ 10.1111/apha.13101.
- [61] Cataldo LR, et al. Prolonged activation of the Htr2b serotonin receptor impairs glucose stimulated insulin secretion and mitochondrial function in MIN6 cells. PLoS One 2017;12:e0170213. https://doi.org/10.1371/journal.pone.0170213.
- [62] Weitz J, Menegaz D, Caicedo A. Deciphering the complex communication networks that orchestrate pancreatic islet function. Diabetes 2021;70:17–26. https://doi. org/10.2337/dbi19-0033.
- [63] Taneera J, et al. gamma-aminobutyric acid (GABA) signalling in human pancreatic islets is altered in type 2 diabetes. Diabetologia 2012;55:1985–94. https://doi.org/ 10.1007/s00125-012-2548-7
- [64] Mills PB, et al. Mutations in antiquitin in individuals with pyridoxine-dependent seizures. Nat Med 2006;12:307–9. https://doi.org/10.1038/nm1366.

- [65] Gospe Jr SM, Olin KL, Keen CL. Reduced GABA synthesis in pyridoxine-dependent seizures. Lancet 1994;343:1133–4. https://doi.org/10.1016/s0140-6736(94) 90236-4
- [66] Pena IA, et al. Mouse lysine catabolism to aminoadipate occurs primarily through the saccharopine pathway; implications for pyridoxine dependent epilepsy (PDE). Biochim Biophys Acta Mol basis Dis 2017;1863:121–8. https://doi.org/10.1016/j. bbadis 2016.09.006
- [67] Pinckaers PJM, et al. No differences in muscle protein synthesis rates following ingestion of wheat protein, milk protein, and their protein blend in healthy, young males. Br J Nutr 2021;126:1832–42. https://doi.org/10.1017/ S0007114521000635.
- [68] Rogers LM, et al. Postprandial plasma aminoacidemia and indices of appetite regulation following pea-rice blend, pea isolate and whey protein ingestion in healthy young adults. Br J Nutr 2024;132:691–700. https://doi.org/10.1017/ S0007114524001958.
- [69] Norrelund H, et al. Abnormalities of whole body protein turnover, muscle metabolism and levels of metabolic hormones in patients with chronic heart failure. J Intern Med 2006;260:11–21. https://doi.org/10.1111/j.1365-2796-2006-0163 x
- [70] Tondo M, et al. Clinical, biochemical, molecular and therapeutic aspects of 2 new cases of 2-aminoadipic semialdehyde synthase deficiency. Mol Genet Metab 2013; 110:231–6. https://doi.org/10.1016/j.ymgme.2013.06.021.
- [71] Xu L, et al. Metabolic profilings of rat INS-1 beta-cells under changing levels of essential amino acids. Sci Data 2022;9:299. https://doi.org/10.1038/s41597-022-01436-w.
- [72] Ewald JD, et al. HumanIslets.com: improving accessibility, integration, and usability of human research islet data. Cell Metab 2024. https://doi.org/10.1016/j. cmet.2024.09.001.